Non-linear transcriptional responses to gradual modulation of transcription factor dosage

Júlia Domingo[1*†], Mariia Minaeva[2,#], John A Morris[1,3], Marcello Ziosi[1], Neville E Sanjana[1,3], Tuuli Lappalainen[1,2*]

1: New York Genome Center, New York, NY 10013, USA.

2: Science for Life Laboratory, Department of Gene Technology, KTH Royal Institute of Technology, Stockholm, Sweden.

3: Department of Biology, New York University, New York, NY 10003, USA.

* Corresponding authors: jdomingo@nygenome.org; tlappalainen@nygenome.org
† Current affiliation: Allostery Exploration Technologies, S.L., Barcelona, Spain.
# Current affiliation: Institute of Computational Biology, Helmholtz Center, Munich, Germany.

Abstract

Genomic loci associated with common traits and diseases are typically non-coding and likely impact gene expression, sometimes coinciding with rare loss-of-function variants in the target gene. However, our understanding of how gradual changes in gene dosage affect molecular, cellular, and organismal traits is currently limited. To address this gap, we induced gradual changes in gene expression of four genes using CRISPR activation and inactivation. Downstream transcriptional consequences of dosage modulation of three master trans-regulators associated with blood cell traits (GFI1B, NFE2, and MYB) were examined using targeted single-cell multimodal sequencing. We showed that guide tiling around the TSS is the most effective way to modulate *cis* gene expression across a wide range of fold-changes, with further effects from chromatin accessibility and histone marks that differ between the inhibition and activation systems. Our single-cell data allowed us to precisely detect subtle to large gene expression changes in dozens of *trans* genes, revealing that many responses to dosage changes of these three TFs are non-linear, including non-monotonic behaviours, even when constraining the fold-changes of the master regulators to a copy number gain or loss. We found that the dosage properties are linked to gene constraint and that some of these non-linear responses are enriched for disease and GWAS genes. Overall, our study provides a straightforward and scalable method to precisely modulate gene expression and gain insights into its downstream consequences at high resolution.

Introduction

Precision control of gene expression levels plays a pivotal role in defining cell type specificity and coordinating responses to external stimuli. Imbalances in this intricate regulation can underlie the genetic basis of both common and rare human disease. The vast majority of

genetic variants associated with complex disease, as revealed by genome-wide association studies (GWAS), are located in noncoding regions, with likely gene regulatory effects [1]. Previous studies have attempted to elucidate these effects by mapping genetic associations to gene expression [2,3], and more recently, CRISPR-based perturbations of GWAS loci have provided insights into their functional consequences [4]. A major driver of rare genetic diseases are loss-of-function variants affecting one or both copies of the gene, leading to disease via dramatic reduction of functional gene dosage [5]. The substantial overlap [6,7] and potential joint effects [8,9] of rare and common variants indicate a general link between different degrees of perturbation of gene dosage and disease phenotypes.

However, our understanding of the quantitative relationship between gradual changes of gene dosage and downstream phenotypes remains elusive for most human genes. Practical applications of the compelling allelic series concept to identify genes where increasingly deleterious mutations have increasing phenotypic effects have been limited by the sparsity of segregating variants with an impact on a given gene in the human population [10]. Experimental characterization of gene function in model systems has predominantly relied on gene knock-out or knock-down approaches [11]. While these studies have proven useful to identify dosage sensitive genes involved in cellular functions and disease [12–16], these approaches only provide a limited discrete relationship between the number of functional gene copies and a certain phenotype (eg. loss-of-function consequence vs. wild-type). However, such relationships are in fact determined by continuous dosage-to-phenotypes functions that, as suggested by a small number of previous experimental studies [17–19], can be complex and thus are challenging to infer from loss-/gain-of-function data.

Recently, new methods have enabled the gradual modulation of gene dosage in model systems [18,20,21], while large-scale insights into the downstream effects of dosage modulation have largely come from yeast [17] and bacteria [19,22], demonstrating that non-linear relationships between gene dosage and phenotype are common. In humans, the relationship between dosage and downstream phenotype is largely unexplored. Only a few limited studies have dissected these consequences, for instance on the disease-associated transcription factor SOX2 [23]. Such work showed a non-linear relationship between dosage and multiple tiers of phenotypes, including DNA accessibility, RNA expression of downstream targets, rending the question if such phenomenon occurs with other transcription factors. More recently, similar evidence has been shown in the case of the NKX2-1 lineage factor with oncogenic role in lung adenocarcinoma [24]. Generally, transcription factors represent a particularly compelling target for characterization of gene dosage effects. They are key regulators of cellular functions, enriched for disease associations[25] and often classified as haploinsufficient [26]. Additionally, their effects can be measured by transcriptome analysis. However, our knowledge of their dosage-dependent effects on regulatory networks still remains limited.

In this study, we developed and characterised a scalable novel approach for gradually decreasing and increasing gene dosage with the CRISPRI inhibition (CRISPRi) and activation (CRISPRa) systems. We applied this to four genes, with single cell RNA-sequencing (scRNA-seq) as a cellular readout of downstream effects. We uncovered a quantitative landscape of how gradual changes in transcription dosage lead to linear and non-linear response in downstream genes, including those associated with rare and complex disease, with potential effects on cellular phenotypes.

Results

Precise modulation and quantification of gene dosage using CRISPR and targeted multimodal single-cell sequencing

We selected four genes for gradual modulation of their dosage in the human erythroid progenitor cell line K562 [27]: *GFI1B*, *NFE2*, *MYB* and *TET2*. Two of the genes, *GFI1B* and *NFE2*, have been implicated in blood diseases and traits [28–30], and in our earlier work we identified a broad transcriptional response to inhibition of GWAS-overlapping enhancers to these genes [4]. *MYB* is a key transcription factor [31] and a downstream target of GFI1B [4].*TET2* has a role in DNA demethylation and is unrelated to these transcriptional networks and is included in this study as control with minimal expected *trans* effects. We refer to these four genes, targeted in *cis* for modulation of their regulation, as *cis* genes (**Figure 1A**).

To modulate the gene expression of the *cis* genes we use K562 cells expressing CRISPRi (KRAB-dCas9-MECP2) and CRISPRa (dCas9-VPR) systems (see Methods), both cell lines hashed with DNA conjugated antibodies against different surface proteins that allow pooled experiments. To obtain a wide range of dosage effects we used four different single guide RNA (sgRNA) design strategies (**Figure 1B**): 1) targeting the transcription start site (TSS) as in the standard CRISPRi/CRISPRa approach, 2) tiling sgRNAs +/- 1000 bp from the TSS, 3) targeting known *cis*-regulatory elements (CREs), and 4) using attenuated guides that target the TSS but contain mismatches to modulate their activity [18]. We further included 5 non-targeting control (NTC) sgRNAs as negative controls.

The library of altogether 96 guides was transduced to a pool of K562-CRISPRi and K562-CRISPRa cells at low multiplicity of infection (MOI). After eight days, we performed ECCITE-seq (see Methods) to capture three modalities: cDNA, sgRNAs and surface protein hashes (oligo-tagged antibodies with unique barcodes against ubiquitously expressed surface proteins). Instead of sequencing the full transcriptome, we used target hybridization to capture a smaller fraction of the cDNA and obtain more accurate expression readouts at a feasible cost. The subset of selected transcripts were picked from the transcriptional downstream regulatory networks of GFI1B and NFE2 identified previously [4], maintaining similar patterns of co-expression correlation across co-expression clusters (see Methods, **Figure S1A**). We targeted a total of 94 transcripts (**Figure 1A**), including the four *cis* genes, 86 genes that represent trans targets of GFI1B and/or NFE2 [4] (**Figure S1A**), *LXH3* that is not expressed in blood progenitors, *GAPDH* that is highly expressed and often considered an invariable housekeeping gene and the dCas9-VPR or KRAB-dCas9-MeCP2 transcripts.

We used the protein hashes and the dCas9 cDNA (the presence or absence of the KRAB domain) to demultiplex and determine the cell line—CRISPRi or CRISPRa—cells containing a single sgRNA per cell were determined using a Gausian mixed model (see Methods). We applied standard QC approaches to the scRNA-seq data and demonstrated the success of the target capture (see Methods, **Figure S1C**). The final data set had 20,001 cells (10,647 CRISPRi and 9,354 CRISPRa), with an average of 81 and 86 cells with a unique sgRNA for the CRISPRa and CRISPRi, respectively (**Figure S1D**).

Gradual modulation of gene expression across a broad range with CRISPRi/a

Next, we calculated the expression fold change for each of the four *cis* genes targeted by each sgRNA in the two cell lines (CRISPRi/a), comparing each group of cells with its respective NTC sgRNA group (see Methods). We first confirmed that the sgRNAs targeting the transcription start site (TSS) up- and down-regulated their targets (**Figure 1C**, **Figure S1F**). When looking at all sgRNAs at once, across the four genes, we observed a 2.3 fold range (**Figure 1E**), with minimum 72% reduction and maximum 174% increased expression (log2(FC) values from -1.83 to 0.80). However, the range varied between the genes, with GFI1B covering the widest range of gene expression changes (gene expression ranging between 0.28 to 1.42 fold), while MYB expression could not be pushed higher than 1.13 fold (**Figure 1E**). The direction of the effects were consistent with the cell lines of origin, where 98.88% of the significant perturbations (Wilcoxon rank test at 10% FDR, n = 89) were correctly predicted based on the direction of the target gene fold change. The predicted on- and off-target properties of the guides [32–34] did not correlate with the fold changes in the *cis* genes (**Figure S2A**), suggesting that the observed effects represent true *cis*-regulatory changes. The fold changes were also robust to the number of cells containing a particular sgRNA (**Figure S2B**, top). Additionally, we verified that the fold change estimation was not biassed depending on the expression level of the target gene at the single-cell level, which can vary due to drop-out effects or binary on/off effects of the KRAB-based CRISPRi system [20]. By splitting cells with the same sgRNA based on the normalised expression of the *cis* gene (0 vs. >0 normalised UMIs, **Figure S2D**), we observed highly concordant transcriptome gene expression effects between the two groups (**Figure S2E**). This indicates that the dosage changes per guide were not primarily driven by the changing frequency of binary on/off effects, and the use of pseudo-bulk fold changes provides a robust estimation of *cis* gene fold changes.

The fold change patterns differed between sgRNA designs (**Figure 1D**, left). As expected, sgRNAs targeting the TSS showed strong perturbations in gene expression. However, sgRNAs tiled +/- 1kb from the TSS provided a broader and more gradual range of up- and downregulation across the target genes, sometimes surpassing the effects of TSS-targeting sgRNAs. Attenuated sgRNAs with mismatch mutations resulted in a range of gene silencing effects in the CRISPRi line, as expected based on their original design [18]. However, these attenuated sgRNAs did not exhibit such a dynamic range in the CRISPRa modality, although a significant correlation existed between the silencing or activating effect size and the distance of the mismatch from the protospacer adjacent motif (PAM) when considering all data points together (**Figure S2C**). The sgRNAs targeting distal *cis*-regulatory elements (CREs) showed both inhibiting and activating effects, even though both the CRISPRi and CRISPRa constructs were initially designed to inhibit or activate transcription from the promoter and initial gene body region. Nonetheless, the number of known CREs per gene is typically limited. Given its simplicity and the ability to achieve both up- and down-regulation of the target gene, we consider the tiling sgRNA approach, with a simple design that only

requires annotation of the TSS, as the best unbiased method for gradually modulating gene dosage with CRISPRi/a systems.

Cis determinants of dosage

Having designed guides targeting both distal and local neighbouring regulatory regions of the four transcription factors (TFs) and ensuring minimal bias in fold-changes due to sgRNA's biochemical properties, we investigated the *cis* features that determine the strength of dosage perturbation. We observed substantial differences in the effects of the same guide on the CRISPRi and CRISPRa backgrounds, with no significant correlation between *cis* gene fold-changes (**Figure 2A**). However, in both modalities, the strongest effects on gene expression were observed when the guides were close to the transcription start site (TSS) (**Figure 2B**, excluding NTC and attenuated sgRNAs), although the peaks of strongest activation or repression differed between the modalities. In the CRISPRi modality, the maximum effect was located within the gene body at +238 bp from the TSS (**Figure 2B**, bottom), consistent with previous studies that used essentiality as a proxy for expression [35]. However, in the CRISPRa modality, the maximum average fold changes occurred closer to the TSS at around -99 bp (**Figure 2B**, bottom), as also shown for CD45 [36].

Enhancer, tiling and TSS sgRNAs targeted regions of the genome with different compositions of histone marks in K562 annotated by ENCODE [37] (**Figure 2C**). This allowed us to investigate the impact of chromatin state on the strength of *cis* gene dosage modulation. The magnitude of *cis* gene fold changes varied significantly depending on the presence of specific marks or peaks, which again differed between the two modalities (**Figure 2D**). In the CRISPRa cell line, the strongest effects were observed when guides were located in regions with open chromatin marks such as DNase or ATAC peaks. In contrast, the strongest repression by CRISPRi occurred in genomic regions with the presence of H3K27ac, H3K4me3, and H3K9ac marks. These differences may be explained by the distinct mechanisms of action of activator and repressor domains. MeCP2 and KRAB repressor domains recruit additional repressors that silence gene expression through chromatin remodelling activities such as histone deacetylation [38]. On the other hand, the VPR activation fusion domain may only require Cas9 to scan the open chromatin and recruit RNA polymerase and additional transcription factors to activate transcription. Overall, while a few sgRNAs have a strong effect in both CRISPRi and CRISPRa cell lines, a single guide library containing guides optimised for both modalities enables a range of gradual dosage regulation. However, larger data sets are needed for more careful modelling of the ideal dosage modulation designs and to understand how both *cis*-regulatory features, feedback loops and other mechanisms contribute to the outcomes.

Trans responses of transcription factor dosage modulation

We then turned our attention to the remaining 91 genes captured by our custom panel and determined the relative expression fold change of each *trans* gene, compared to NTC in each unique guide perturbation (see Methods). Principal component analysis (PCA) performed on all pseudo-bulk fold changes demonstrated the removal of batch effects from

the cell lines and revealed a clear direction of the *cis* gene dosage effect in the first three principal components (**Figure S3B**). This finding suggests that dosage modulation is the primary determinant of *trans* effects, explaining approximately 60% of the variance. Additionally, the PCA indicated that the dosage modulation of GFI1B generally leads to opposite *trans* effects compared to MYB (opposite directions in PC1 and PC2), while the *trans* responses of NFE2 are less related to the previous two TFs, with dosage effects reflected in PC3.

Using a false discovery rate (FDR) cutoff of 0.05, all 91 *trans* genes except the neural specific TF LHX3 (negative control) exhibited a significant change in expression upon perturbation of any of the TFs. Among all measured fold changes, the most extreme negative effect sizes were observed in *cis* genes, with the top 10 being predominantly reductions in GFI1B expression. This indicates that *cis* downregulation tended to surpass the endogenous expression limits. In contrast, the largest increases in gene expression were observed through *trans* mechanisms, where KLK1 and TUBB1 reached the largest expression values when GFI1B was strongly upregulated, or SPI1 and DAPK1 when GFI1B was strongly downregulated. These findings suggest that the CRISPRa approach did not reach a biological ceiling of overexpression.

Inspecting *trans* responses as a function of *cis* gene modulation, we observed that the number of expressed genes and the mean absolute expression changes of *trans* genes exhibited correlations gene-specific correlations with *cis*-gene dosage (**Figure 3A**, **Figure S3C**). Perturbations in GFI1B led to the most pronounced *trans* responses, with positive dosage changes resulting in larger effect sizes compared to decreasing TF gene expression, where the effect plateaued. NFE2 exhibited similar patterns but with smaller magnitude. In the case of MYB, *trans* responses were observed when decreasing the expression of this TF, but the effects of upregulation are largely unknown as we were unable to increase MYB expression beyond 0.35. As expected, given the unrelatedness of TET2 to the *trans* network, dosage modulation of this gene had minimal *trans* effects with the least pronounced trend when compared to TET2 dosage, so we excluded it from subsequent analyses.

Widespread non-linear dosage responses in *trans* regulatory networks

Upon clustering the changes in expression of *trans* genes based on the *cis* gene dosage change linked to each sgRNA, we identified distinct clusters exhibiting different dosage-response patterns (**Figure 3B** for GFI1B, **Figure S4-7A** for all *cis* genes). Further examination of the gene expression fold changes for each individual transgene in relation to the TF fold changes revealed a diverse range of response patterns (**Figure 3C**, **Figure S4-7B** for all *cis* genes). These responses exhibited both linear and nonlinear forms, including some instances of non-monotonic gene expression responses for certain *trans* genes within the GFI1B trans network (e.g., GATA2 in **Figure 3C**, **Figure S8E**).

To accurately characterise the dosage response, we employed both linear and nonlinear modelling approaches (**Figure 3D**), which allowed us to quantitatively assess the extent of nonlinear responses by comparing the goodness of fit of these models using the Akaike

Information Criterion (AIC). For the nonlinear model, we utilised a sigmoid function with four free parameters (**Figure 3D**, right). These parameters represented the slope at the inflection point (*b*, indicating the rate of increase or decrease in expression), the minimum and maximum asymptotes (*c* and *d*, representing the lower and upper limits of fold change), and the value of *cis* gene expression at which the inflection point occurs (*a*). To prevent overfitting, we implemented a 10-fold cross-validation scheme, which yielded reliable predictions on the left-out data (pearson r = 0.71 to 0.88 for all *trans* genes in the GFI1B, MYB, and NFE2 networks, **Figure S8C**). Additionally, the predicted parameter *a* was centred around zero, as expected since the input data represents relative fold changes (**Figure S9**). Since a sigmoid function cannot capture non-monotonic responses, we employed a loess regression as an alternative approach for the few genes that exhibited non-monotonic responses (see Methods, **Figure S8D,E**). For the vast majority of genes, the sigmoid (or loess) fit was remarkably good, partially due to the low level of noise in the targeted scRNA-seq data.

We compared the performance of the linear vs. nonlinear models with the ΔAIC ($AIC_{linear} - AIC_{nonlinear}$), where positive ΔAIC means that the sigmoid model captures better the variance in the dosage response than the linear model. This showed that most GFI1B-dependent dosage expression responses are better fit by the sigmoid model (median ΔAIC = 18.7, with 70.4% of all *trans* genes with a significant response having ΔAIC >2, **Figure 3D**). The responses to dosage modulation of MYB and NFE2 were also better captured by the nonlinearities, but towards less extent (0.14 and 3.4 median ΔAIC, with 20.8% and 40.7% of all *trans* genes dosage responses having ΔAIC > 2 for MYB and NFE2, respectively, **Figure S8A**). When ignoring those genes classified as unresponsive (genes that their expression did not change upon the TF modulator, see Methods), even more responses of the remaining *trans* genes were better explained by a sigmoidal model with 83.6%, 26.3% and 63.2% of these having a ΔAIC > 2, for GFI1B, MYB and NFE2 respectively. A similar trend holds even when limiting the models to be fitted to those data points that correspond to a hypothetical one copy loss or gain of the *cis* gene (**Figure S8B**), where the median ΔAIC of responsive genes are 7.05, 0.05 and 3.6 for GFI1B, MYB and NFE2 *trans* responses. Overall this shows that *trans* responses to TF dosage are dominated by nonlinear behaviours even when the TF dosage changes are not extreme but within biologically plausible ranges.

Gene and transcriptional network properties of dosage response

Utilising a model that effectively captures the variance in our data provided the ability to predict unmeasured TF dosage points and facilitated a direct comparison of *trans* effects across different cis genes. Employing the sigmoid model (and loess for those with non-monotonic responses), we estimated the continuous expression of *trans* genes on a uniform fold-change scale across the spectrum of GFI1B, MYB, and NFE2 expression changes (**Figure 4A**). This estimation was carried out within the empirically observed range of all three *cis* genes, spanning from log2(FC) -1.83 to 0.51. Subsequent hierarchical clustering of *trans* gene responses revealed six major clusters of distinct response patterns. For the majority of *trans* genes, the response to GFI1B and MYB was opposite, with only two

small clusters displaying exceptions. Notably, GFI1B generally induced the most substantial response, while NFE2 triggered the smallest range of *trans* gene response.

Next, we collected diverse annotations for the *trans* genes to explore the connections between their regulatory properties, disease associations, and selective constraints concerning their response to TF dosage (**Figure 4B, C**). To quantify these relationships, we assessed significant differences in belonging to these qualitative annotations using the Wilcoxon rank test (**Figure 4D**) and correlated parameters from the sigmoid model with quantitative gene metrics (**Figure 4E**). We hypothesised that genes with annotated selective constraint, numerous regulatory elements, and central positions in regulatory networks would exhibit greater robustness to TF changes. Indeed, housekeeping genes demonstrated a considerably smaller dosage response range (**Figure 4F**). Moreover, genes classified as unresponsive were enriched in the housekeeping category (odds ratio = 2.14, Fisher test p-value = 0.024). The connection between constraint metrics and response properties was also evident in the MYB *trans* network, where the probability of haploinsufficiency (pHaplo) exhibited a significant negative correlation with the range of transcriptional responses of those *trans* genes (**Figure 4G**). However, this result was not reproduced with among the other *trans* networks (**Figure 4E**).

While we observed some strong signals on how the response of *trans* genes similarly vary given similar intrinsic gene properties, most of these differed between GFI1B, MYB and NFE2 *trans* network responses. We also performed a similar analysis comparing the sigmoid parameters to network properties using the approach in [39], obtaining inconsistent results between TF regulons (**Figure S10A, B**). This suggests that the link between commonly annotated gene properties and the responses that the genes have are complex and highly context specific, as in our data from a single cell line, they differed between the upstream regulators that were manipulated. Thus, much more data is needed before transcriptional responses can be predicted from gene properties, and conversely to understand the cellular mechanisms that lead to the annotated gene properties.

Nonlinear dosage responses in complex traits and disease

Moving beyond the characterization of mechanisms of transcriptome regulation, a key question is how gradual dosage variation links to downstream cellular phenotypes, and whether these responses exhibit analogous nonlinear patterns. To address this question, we correlated our findings with the expression profiles of various cell types in order to study the myeloid differentiation process, a phenotype well characterised for our K562 model that has been used as a reliable system for investigating erythroid differentiation within myeloid lineages [40] and blood tumours [41]. Specifically, leveraging single-cell expression data for bone marrow cell types from the Human Cell Atlas and Human Biomolecular Atlas Project [42], we filtered the expression data to the targeted genes in our study. After aggregating data across donors and normalising expression across cell types (**Figure S11A**), we compared the expression patterns resulting from each unique transcription factor dosage modulation in relation to each unique cell type expression state. The ensuing correlation can then be construed as a "phenotype," signifying the similarity between the transcriptional state induced by the TF increase or decrease and the transcriptional state of a specific blood lineage cell type.

Such analyses recapitulate known biology, with GFI1B upregulation [28] and MYB downregulation [43] being crucial factors promoting erythrocyte maturation (**Figure 5A**). The downregulation of NFE2 instead was negatively related to platelet differentiation. Analysing the correlations as inferred phenotypes suggests potential non-linear relationships (**Figure S11B**), but these trends should be considered hypotheses that require experimental validation. In summary, this points to cellular phenotypes resulting from gradual TF dosage modulation.

Many of the analysed *trans* genes are associated with physiological traits and diseases (**Figure 4**). Understanding the nonlinear trends in the expression of these genes are of particular interest: It helps us comprehend how these genes with physiological impacts may be buffered against upstream regulatory changes, and how their dosage changes as a response to upstream regulators contrasts with genetic variants that contribute to diseases and traits. Additionally, knowing the underlying dosage-to-phenotype curve of a gene can be crucial if this is considered a biomarker for identifying or treating disease. To investigate this, we analysed whether OMIM genes for rare diseases and Mendelian traits or GWAS genes for different blood cell traits (**Figure 5B**) that are part of the *trans* networks of genes affected by GFI1B, MYB or NFE2 perturbation are enriched for non-linear dosage responses. As seen in **Figure 4**, the *trans* response properties of each gene are highly specific to the regulators and thus analysed in parallel for each *cis* gene network. An enrichment for nonlinear responses was observed for MYB *trans* network genes associated with disease and for blood traits related to white blood cells and reticulocytes. These enrichments are particularly interesting given that most *trans* genes that were sensitive to MYB dosage modulation did not respond with a non-linear trend (**Figure S8A**).

Despite non-linear responses not being significantly enriched among disease genes across all *trans* networks, the responses of the same *trans* gene can show very different dosage responses depending on the upstream regulator being tuned. In **Figure 5C** we show a few examples of genes associated with diseases (1 or more disease phenotypes [44]): FOXP1 is a haploinsufficient and potentially triplosensitive transcription factor associated with intellectual disability; yet it shows a strong response especially to GFI1B dosage across a wide range. NF1A is a haploinsufficient developmental disorder gene with a similar response pattern. However, it is difficult to interpret their expression response in K562 cells when their most apparent phenotypic effects likely derive from other cell types. RHB is the Rhesus blood type gene where a common deletion of the gene causes the Rh- blood type in homozygous individuals, with a strong nonlinear response to GFI1B levels. A particularly interesting gene is TUBB1, part of β-tubulin, that causes autosomal dominant macrothrombocytopenia or abnormally large platelets. Here, K562 cells are a reasonable model system, being closely related precursors to megakaryocytes that produce platelets. Interestingly, GFI1B loss also causes a macrothrombocytopenia phenotype in mice [45], and in our data TUBB1 expression decreases quickly as a function of decreased GFI1B expression but then plateaus at a level that corresponding to loss of one copy of TUBB1. This raises the hypothesis that low GFI1B levels may cause macrothrombocytopenia at least partially via reducing TUBB1 expression.

Discussion

In this paper, we have investigated how gradual dosage modulation of transcription factors contributes to dosage-sensitive transcriptional regulation and investigated its potential phenotypic consequences. First, we set up an easily scalable and generalizable CRISPRi/CRISPRa approach with tiling sgRNAs for gradual titration of gene expression levels, obtaining an informative range and granularity of dosage modifications. However, this approach is not without caveats, as exemplified by our inability to substantially increase MYB expression. Further work and larger *cis* gene sets will be needed to fully understand how widespread this is and to which extent this depends on *cis*-regulatory properties versus feedback and buffering mechanisms. Nevertheless, we believe that the approach proposed here is a useful complement to the diversifying set of tools for dosage modulation for different purposes [18–21].

In this work, we made use of targeted transcriptome sequencing to avoid complications from the sparsity of single cell data. While highly accurate targeted readout of the *cis* gene expression linked to each sgRNA is a core component of our approach, analysing *trans* responses could also be achieved by standard single cell sequencing of the full transcriptome, possible in combination with a targeted readout of transcripts of particular interest. In this study, the targeted genes were selected based on prior data of responding to GFI1B, NFE2 or MYB regulation and thus do not represent an unbiased or random sample of genes.

Our results show that nonlinear responses to gradual up- and downregulation of TF dosage are widespread and that the patterns of transcriptional responses are highly context-specific and vary between upstream regulators. Further work with larger sets of *cis* and *trans* genes as well as direct quantification of cellular readouts will be needed to fully characterise the patterns and mechanisms of downstream impacts on gene dosage. However, our findings indicate important directions for future research. Firstly, the widespread nonlinearity suggests that interpolation or extrapolating gene function assessments from classical molecular biology approaches with drastic knock-outs or knock-downs may have limitations, as their effects can be quantitatively and qualitatively different than more modest perturbations that typically occur in nature. This may be particularly relevant for essential and highly dosage-sensitive genes, where applying our gradual dosage modulation framework can provide opportunities for functional characterization at perturbation levels that do not kill the cells. Secondly, we show that the effects of up- and downregulation are qualitatively and quantitatively different, which calls for increased attention to analysing both directions of effect, which also occur in natural responses to genetic variants and environmental stimuli.

Gene dosage sensitivity has typically been studied by human genetics and genomics methods [46–48]. The experimental approach pursued in this study and the computational approaches are fundamentally different and complement each other: while human genetics is powerful for capturing functional importance on physiological phenotypes via patterns of contemporary population variation and selective constraint, experimental approaches provide more granularity and insights into cellular mechanisms. Furthermore, while the

convergence of disease effects of common and rare variants affecting the same gene is a well-known phenomenon [6,7], the sparsity of variants makes it difficult to properly model allelic series as a continuous dosage-to-phenotype function for individual genes. Experimental approaches can provide a powerful complement to this. Altogether, we envision that combining these perspectives into true systems genetics approaches will be a powerful way to understand how gene dosage variation contributes to human phenotypes from molecular to cellular and eventually physiological levels.

Acknowledgments

This work was funded by NIH grants R01MH106842, R01AG057422, DP2HG010099, R01HG012790, and R01GM122924; a grant from the Knut and Alice Wallenberg Foundation to SciLifeLab for research in Data-driven Life Science, DDLS (KAW 2020.0239); funding from the European Research Council (ERC) under the European Union's Horizon 2020 research and innovation programme (Grant agreement No. 101043238); a European Molecular Biology Organization Postdoctoral Fellowship (ALTF 345-2021) to J.D.; a Canadian Institutes of Health Research Banting Postdoctoral Fellowship and NIH/NHGRI (K99HG012792) to J.A.M.

Competing Interests:

J.D. is CEO and co-founder with equity in Allostery Exploration Technologies, S.L. T.L. was a paid advisor to GSK, and is an advisor and has equity in Variant Bio.

Author Contributions

J.D. and T.L. conceived the study. J.D. performed the experiments, with contributions from J.A.M. and M.Z.. N.S. contributed experimental resources to the study. J.D. performed the computational analyses, with contributions from M.M. and J.A.M.. J.D. and T.L. wrote the manuscript with contributions and review from all the authors.

Data availability and materials

All code used in this study is available at https://github.com/LappalainenLab/d2n_ms. Raw sequencing data has been submitted to GEO (accession number GSE257547).

References

1. Maurano, M. T. *et al.* Systematic localization of common disease-associated variation in regulatory DNA. *Science* **337**, 1190–1195 (2012).

2. GTEx Consortium. The GTEx Consortium atlas of genetic regulatory effects across

human tissues. *Science* **369**, 1318–1330 (2020).

3. Claussnitzer, M. *et al.* A brief history of human disease genetics. *Nature* **577**, 179–189 (2020).
4. Morris, J. A. *et al.* Discovery of target genes and pathways at GWAS loci by pooled single-cell CRISPR screens. *Science* **380**, eadh7699 (2023).
5. Zschocke, J., Byers, P. H. & Wilkie, A. O. M. Mendelian inheritance revisited: dominance and recessiveness in medical genetics. *Nat. Rev. Genet.* **24**, 442–463 (2023).
6. Backman, J. D. *et al.* Exome sequencing and analysis of 454,787 UK Biobank participants. *Nature* **599**, 628–634 (2021).
7. Freund, M. K. *et al.* Phenotype-Specific Enrichment of Mendelian Disorder Genes near GWAS Regions across 62 Complex Traits. *Am. J. Hum. Genet.* **103**, 535–552 (2018).
8. Castel, S. E. *et al.* Modified penetrance of coding variants by cis-regulatory variation contributes to disease risk. *Nat. Genet.* **50**, 1327–1334 (2018).
9. Fahed, A. C. *et al.* Polygenic background modifies penetrance of monogenic variants for tier 1 genomic conditions. *Nat. Commun.* **11**, 3635 (2020).
10. McCaw, Z. R. *et al.* An allelic-series rare-variant association test for candidate-gene discovery. *Am. J. Hum. Genet.* **110**, 1330–1342 (2023).
11. Sanjana, N. E. Genome-scale CRISPR pooled screens. *Anal. Biochem.* **532**, 95–99 (2017).
12. Collins, R. L. *et al.* A cross-disorder dosage sensitivity map of the human genome. *medRxiv* (2021).
13. Fehrmann, R. S. N. *et al.* Gene expression analysis identifies global gene dosage sensitivity in cancer. *Nat. Genet.* **47**, 115–125 (2015).
14. Wang, T. *et al.* Identification and characterization of essential genes in the human genome. *Science* **350**, 1096–1101 (2015).
15. Hart, T. *et al.* High-Resolution CRISPR Screens Reveal Fitness Genes and Genotype-Specific Cancer Liabilities. *Cell* **163**, 1515–1526 (2015).
16. Cowley, G. S. *et al.* Parallel genome-scale loss of function screens in 216 cancer cell

lines for the identification of context-specific genetic dependencies. *Sci Data* **1**, 140035 (2014).

17. Keren, L. *et al.* Massively Parallel Interrogation of the Effects of Gene Expression Levels on Fitness. *Cell* vol. 166 1282–1294.e18 Preprint at https://doi.org/10.1016/j.cell.2016.07.024 (2016).
18. Jost, M. *et al.* Titrating gene expression using libraries of systematically attenuated CRISPR guide RNAs. *Nat. Biotechnol.* **38**, 355–364 (2020).
19. Hawkins, J. S. *et al.* Mismatch-CRISPRi Reveals the Co-varying Expression-Fitness Relationships of Essential Genes in Escherichia coli and Bacillus subtilis. *Cell Syst* **11**, 523–535.e9 (2020).
20. Noviello, G., Gjaltema, R. A. F. & Schulz, E. G. CasTuner is a degron and CRISPR/Cas-based toolkit for analog tuning of endogenous gene expression. *Nat. Commun.* **14**, 3225 (2023).
21. Chiarella, A. M. *et al.* Dose-dependent activation of gene expression is achieved using CRISPR and small molecules that recruit endogenous chromatin machinery. *Nat. Biotechnol.* **38**, 50–55 (2020).
22. Lalanne, J.-B., Parker, D. J. & Li, G.-W. Spurious regulatory connections dictate the expression-fitness landscape of translation factors. *Mol. Syst. Biol.* **17**, e10302 (2021).
23. Naqvi, S. *et al.* Precise modulation of transcription factor levels identifies features underlying dosage sensitivity. *Nat. Genet.* (2023) doi:10.1038/s41588-023-01366-2.
24. Pulice, J. L. & Meyerson, M. Dosage amplification dictates oncogenic regulation by the NKX2-1 lineage factor in lung adenocarcinoma. *bioRxiv* (2023) doi:10.1101/2023.10.26.563996.
25. Mostafavi, H., Spence, J. P., Naqvi, S. & Pritchard, J. K. Systematic differences in discovery of genetic effects on gene expression and complex traits. *Nat. Genet.* **55**, 1866–1875 (2023).
26. van der Lee, R., Correard, S. & Wasserman, W. W. Deregulated Regulators: Disease-Causing cis Variants in Transcription Factor Genes. *Trends Genet.* **36**,

523–539 (2020).

27. Ulirsch, J. C. *et al.* Systematic Functional Dissection of Common Genetic Variation Affecting Red Blood Cell Traits. *Cell* **165**, 1530–1545 (2016).
28. Möröy, T., Vassen, L., Wilkes, B. & Khandanpour, C. From cytopenia to leukemia: the role of Gfi1 and Gfi1b in blood formation. *Blood* **126**, 2561–2569 (2015).
29. Polfus, L. M. *et al.* Whole-Exome Sequencing Identifies Loci Associated with Blood Cell Traits and Reveals a Role for Alternative GFI1B Splice Variants in Human Hematopoiesis. *Am. J. Hum. Genet.* **99**, 481–488 (2016).
30. Jutzi, J. S. *et al.* Altered NFE2 activity predisposes to leukemic transformation and myelosarcoma with AML-specific aberrations. *Blood* **133**, 1766–1777 (2019).
31. Baker, S. J. *et al.* B-myb is an essential regulator of hematopoietic stem cell and myeloid progenitor cell development. *Proc. Natl. Acad. Sci. U. S. A.* **111**, 3122–3127 (2014).
32. Doench, J. G. *et al.* Rational design of highly active sgRNAs for CRISPR-Cas9-mediated gene inactivation. *Nat. Biotechnol.* **32**, 1262–1267 (2014).
33. Doench, J. G. *et al.* Optimized sgRNA design to maximize activity and minimize off-target effects of CRISPR-Cas9. *Nat. Biotechnol.* **34**, 184–191 (2016).
34. McKenna, A. & Shendure, J. FlashFry: a fast and flexible tool for large-scale CRISPR target design. *BMC Biol.* **16**, 74 (2018).
35. Sanson, K. R. *et al.* Optimized libraries for CRISPR-Cas9 genetic screens with multiple modalities. *Nat. Commun.* **9**, 5416 (2018).
36. Legut, M. *et al.* High-Throughput Screens of PAM-Flexible Cas9 Variants for Gene Knockout and Transcriptional Modulation. *Cell Rep.* **30**, 2859–2868.e5 (2020).
37. Luo, Y. *et al.* New developments on the Encyclopedia of DNA Elements (ENCODE) data portal. *Nucleic Acids Res.* **48**, D882–D889 (2020).
38. Lupo, A. *et al.* KRAB-Zinc Finger Proteins: A Repressor Family Displaying Multiple Biological Functions. *Curr. Genomics* **14**, 268–278 (2013).
39. Minaeva, M., Domingo, J., Rentzsch, P. & Lappalainen, T. Specifying cellular context of transcription factor regulons for exploring context-specific gene regulation programs.

bioRxiv 2023.12.31.573765 (2024) doi:10.1101/2023.12.31.573765.

40. Wang, H. *et al.* Dynamic transcriptomes of human myeloid leukemia cells. *Genomics* **102**, 250–256 (2013).
41. Salvadores, M., Fuster-Tormo, F. & Supek, F. Matching cell lines with cancer type and subtype of origin via mutational, epigenomic, and transcriptomic patterns. *Sci Adv* **6**, (2020).
42. Granja, J. M. *et al.* Single-cell multiomic analysis identifies regulatory programs in mixed-phenotype acute leukemia. *Nat. Biotechnol.* **37**, 1458–1465 (2019).
43. Jayapal, S. R. *et al.* Down-regulation of Myc is essential for terminal erythroid maturation. *J. Biol. Chem.* **285**, 40252–40265 (2010).
44. Amberger, J. S., Bocchini, C. A., Schiettecatte, F., Scott, A. F. & Hamosh, A. OMIM.org: Online Mendelian Inheritance in Man (OMIM®), an online catalog of human genes and genetic disorders. *Nucleic Acids Res.* **43**, D789–98 (2015).
45. Beauchemin, H. *et al.* Gfi1b controls integrin signaling-dependent cytoskeleton dynamics and organization in megakaryocytes. *Haematologica* **102**, 484–497 (2017).
46. Collins, R. L. *et al.* A structural variation reference for medical and population genetics. *Nature* **581**, 444–451 (2020).
47. Mohammadi, P. *et al.* Genetic regulatory variation in populations informs transcriptome analysis in rare disease. *Science* **366**, 351–356 (2019).
48. Dong, D. *et al.* An RNA-informed dosage sensitivity map reflects the intrinsic functional nature of genes. *Am. J. Hum. Genet.* **110**, 1509–1521 (2023).

STAR Methods

Experimental methods

Plasmids, bacteria strains and cell lines used

Plasmids

- pCC_05: Lentiviral Puromycin CRISPRa dCas9-VPR system (Addgene 139090)
- pGC02: Lentiviral Blasticydin plasmid with CRISPRi KRAB-dCas9-MeCP2 system (Addgene 170068)
- pJDE003: Lentiviral Blasticydin CRISPRa dCas9-VPR system (this study)
- pGC03: Lentiviral Puromycin sgRNA library cloning vector (Addgene 170069)
- pMD2G: Lentiviral envelope plasmid (Addgene 12259)
- psPAX2: Lentiviral packaging plasmid (Addgene 12260)
-

Bacteria *E.coli* strains

- 5-alpha competent cells (NEB C2987H)
- One Shot Stbl3 competent cells (Invitrogen 1934665)
- Endura electrocompetent cells (Lucigen 60242-2)

Cell lines:

- HEK293FT (Thermo Fisher Scientific R70007); cells were maintained at 37℃ and 5% CO2 in high glucose DMEM (Cytiva SH30022.01) supplemented with 10% Serum Plus II (Sigma-Aldrich 14009C)
- K562 (ATCC, CCL243);
  Cells were maintained at 37℃ and 5% CO2; HEK293FT were cultured in high glucose DMEM (Cytiva SH30022.01) supplemented with 10% Serum Plus II (Sigma-Aldrich 14009C); K562 were cultured in IMDM, GlutaMAX (Thermo Scientific 31980097) supplemented with 10% Serum Plus II.

CRISPRa vector construction

To construct the vector harbouring the CRISPRa system (pJDE003), the CRISPRi (KRAB-dCas9-MeCP2) gene fusion of pGC02 [1] was replaced with dCas9-VPR cassette, which was PCR amplified (Q5 High-Fidelity 2X Master Mix, NEB M0492L) from the plasmid pCC_05 [2] with primers oJDE005 and oJDE006 following instructions from manufacturer. pGC02 was digested with XbaI-FD and BamHI-FD (Thermo Fisher FD0685 and FD0054) and sequentially dephosphorylated with FastAP (Thermo Fisher EF0651) following the manufacturer's recommendations. The digested pGC02 vector and the PCR insert with the CRISPRa system (previously treated with a 15 min DpnI enzyme incubation, Thermo Fisher FD1704) were assembled by Gibson assembly using a 2:1 insert:vector ratio with Gibson Assembly Master Mix (NEB E2611S). Assemblies were transformed into NEB 5-alpha *E.coli* competent cells and single colonies were picked and sequence validated by Sanger

sequencing. Frozen stock of the correct construct cells were regrown for plasmid Maxiprep extraction (QIAGEN 12362) for subsequent virus production.

CRISPRa K562 cell line construction and functional validation

Lentivirus was produced by polyethylenimine linear MW 25000 (Polysciences 23966) transfection of HEK293FT cells with the transfer plasmid containing a Cas9-VPR effector, packaging plasmid psPAX2 (Addgene 12260) and envelope plasmid pMD2.G (Addgene 12259). After 72 h post-transfection, cell media containing lentiviral particles was harvested and filtered through 0.45 µm filter Steriflip-HV (Millipore SE1M003M00). One volume of Lentivirus Precipitation Solution (Alstem VC100) was added to the collected lentivirus, mixed and stored overnight at 4C. The mix was centrifuged for 30 min at 1,500g, and the pellet of lentiviral particles were resuspended in 1/10th of the original volume of DMEM media. Lentivirus vials were frozen at -80C and later thawed for transduction.

To construct the monoclonal K562 cell line with the CRISPRa system, the dCas9-VPR lentivirus was transduced into one million K562 cells using 100 µl of 10X concentrated lentivirus in a total volume of 1 ml (high MOI). After 24 hours, the media was replaced with fresh IMDM, and 48 hours after transduction, blasticidin (A.G. Scientific B-1247) was added to a final concentration of 10 µg/µl for 16 days. Monoclonal cell lines were sorted by FACS (Sony Cell Sorter SH800) into a 96-well plate. The presence of dCAS9 protein in several growing clones was confirmed by western blot (Primary antibody: Purified anti-CRISPR CAS9 antibody; BioLegend 844302. Secondary antibody: LI-COR 925-32212) and protein levels were normalised to GAPDH (Primary antibody: GAPDH (14C10) Rabbit; Cell Signalling Technology 2118S. Secondary antibody: LI-COR 925-68073).

To select the final monoclonal CRISPa cell line, the three clones with the highest protein expression in the western blot were subjected to functional validation to test for activation activity. Lentiviral guides designed from [2] targeting CD4 (Anti-CD4 Mouse Monoclonal Antibody (FITC), BioLegend, 300505), which is lowly expressed in K562, CD19 (Anti-CD19 Mouse Monoclonal Antibody (APC),BioLegend, 302211) with null expression, and CD45 (PE anti-human CD45, BioLegend, 368509) with intermediate expression, were independently transduced into all three monoclonals, and after puromycin selection, the expression of this markers was screened by FACS at day 4 and at day 10 or 11 after transduction. The clone with the strongest and most consistent activity was selected.

Gene selection for targeted sequencing and design of probe custom panel

The four selected dosage genes were GFI1B, NFE2, MYB, and TET2. GFI1B and NFE2 were chosen due to their reported trans effects following the inhibition of their cis-CREs [3]. MYB was selected for being downstream of the GFI1B network, and TET2 was selected as an unrelated gene to those transcriptional networks. Both MYB and TET2 qualified as oncogene and tumour suppressor functions in K562 (https://depmap.org/portal/), making them ideal choices to determine the impact of growth effects on the experiment.

The additional 88 genes captured by targeted sequencing were selected based on the significant trans effects of GFI1B and NFE2 inhibition from [3] including two control genes, GAPDH, and LHX3 genes, one highly constantly expressed "housekeeping gene" and the other with no reported expression in K562 cell lines, respectively. The remaining 86 genes were selected based on Morris et al. to include 1) 29 genes that overlapped between the NFE2 and GFI1B network, 2) 47 trans genes for GFI1B, 10) trans genes for NFE2. The number of trans genes selected from each unique network was proportionally chosen, given the size of each trans network, and oversampling TFs and TF targets as defined in [4], as well as maintaining the proportional co-expression cluster structure as defined in [3] (**Figure S1a,b**). Additional filters in the selection included a minimum expression of 0.1 mean UMI/cell and the lack of alternative 5' splice isoforms and a unique Ensembl ID.

The 10X Probe Full Custom Panel design tool was used to design the targeted gene expression probe library. A total of 687 probes (~15%) were discarded because they covered transcript regions with a median coverage per base of < 3 reads/bp (for medium and highly expressed genes) or <1 reads/bp (for lowly expressed genes). All probes for LHX3 (0 median reads/bp) were retained. In addition, 93 probes covering the entire transcript sequence of the dCas9-VPR and KRAB-dCas9-MeCP2 transcript were included, resulting in a final total of 4,405 probes. The xGen™ Custom Hybridization Capture Panel of biotinylated oligos was ordered and synthesised at IDT.

Gene dosage sgRNA library design and cloning

The sgRNA library contained a total of 96 guides (51 tiling, 8 TSS, 20 attenuated, 12 enhancer and 5 non-targeting controls). All guides were designed to not contain the U6 terminator sequence, repeats of five or more consecutive G, C or As, as well as not falling in the genomic region where K562 cell line has alternative alleles compared to the human genome reference (Hg38). All guides were scored with FlashFry [5] to obtain off-target and on-target activity scores that allowed the selection of the best scoring guides. Tiling guides were designed to target different regions of the promoter, TSS and beginning of the gene body of each dosage gene, spanning a total average distance of 1400 bp (TSS in the centre), each being on average distant from one another of 110 bp. The sequences of the two TSS guides were obtained from [6]. The sgRNAs targeting enhancers were picked from previously reported work that showed a CRISPR-based evidence of enhancer activity (GFI1B [1], NFE2 [7], MYB [8]). The five attenuated guides for each gene were manually designed following the rules described in [9] to span a range of activities, including a single point mutation on the best scoring guide that targeted the TSS.

Overhangs with homology regions to the pGC03 plasmid (18bp downstream and 22 bp upstream) were added to the sgRNA sequence to be able to directly clone the ssDNA oligos into the plasmid. The 96 sgRNAs were ordered in IDT as single stranded DNA oligos (total 60bp) in a 96 well-plate to 100 pmol scale. The oligos were pooled at equimolar concentration and diluted to a final concentration of 0.2 uM. The library was cloned into the BsmBI digested plasmid pGC03 using 10 reactions of the NEBuilder HiFi DNA Assembly kit following the manufacturer's instructions. All the reactions were pooled and the DNA precipitated using Isopropanol, GlycoBlue (Thermo Scientific AM9515) and 50mM NaCl for

15 min at RT. Following two washes with Ethanol 70%, the assembly was resuspended with 15ul of 0.2X TE.

To transform the library into E.coli, 1ul of the assembly was mixed with 25 uL of Endura cells under manufacturer's electroporation conditions, then plated onto 245 x 245 mm square LB 100 ug/ml Carbenicillin plates. The plates were grown ON, and >2.5e5 transformants were obtained, ensuring the complexity of the library was maintained at >1000 cells per unique sgRNA. All colonies were collected and subjected to maxiprep using the Maxi Fast-Ion Plasmid Kit, Endotoxin Free kit (IBI Scientific IB47123). The representation of the library was assessed through MiSeq shallow sequencing (Illumina).

sgRNA lentiviral library production and cell culture assay

The lentiviral library was produced by transfecting ~80 million HEK293FT cells with a transfer plasmid containing the 96 sgRNA library, along with the packaging plasmid psPAX2 and envelope plasmid pMD2.G, using polyethylenimine linear MW 25000. The supernatant media was replaced with fresh D10 10% BSA six hours after transfection, and the virus was collected and filtered through 0.45 µm filters after 48 hours. The lentiviral library was then concentrated 2X using the Precipitation Lentiviral Solution, aliquoted, and stored at -80°C for subsequent transduction.

Both CRISPRi and CRISPRa K562 cell lines were independently transduced with different titers of the lentiviral sgRNA library at a low MOI (one sgRNA per cell). Twenty hours post-transduction, the cell media was replaced with fresh IMDM 10% Serum Plus II Blasticidin 5 µg/mL, and four hours later, Puromycin (Invivogen ant-pr-1) was added at a final concentration of 2 µg/mL to select for cells with sgRNA integration. The transduction batch with an infection rate of ~10% was selected, and cells were sorted to near purity using FACS to remove dead cells. Cells were maintained at >90% survival and a maximum confluency of 700,000 cells/mL. On day 8 post-transduction, the cells were collected and prepared for cell hashing.

Multimodal single-cell experiment and targeted sequencing

Cell hashing was performed as previously described using four hashtag-derived oligonucleotides (HTOs) in a hyperconjugation protocol [10]. Each transduced cell line was split into four batches of 500,000 cells, resulting in a total of 8 different hashes. After incubation and washes, all 8 hashed batches were pooled together and run in two reaction lanes of the 10X Chromium Next GEM Single Cell 5' Reagent Kit v2 (single indexing, PN-1000265 and PN-1000190). The manufacturer's protocol was followed with modifications stipulated in the ECCITE-seq protocol [11]. For each GEM reaction, 42,000 cells from the hash pool were used to obtain approximately 21,000 total cells, including "multiplets" (multiple cells per droplet counts). Gene expression (cDNA), hashtags (HTOs), and guide RNA (Guide-derived oligos, GDOs) libraries were constructed following the 10x Genomics and ECCITE-seq protocols (https://cite-seq.com/eccite-seq/) with minimal modifications. Specifically, the antibody pool protein tag library steps were ignored, and a custom-designed probe library was used to enrich the cDNA for the genes of interest in the 10X Targeted

Gene Expression protocol (10X PN-1000248). The resulting libraries were sequenced using an Illumina Nextseq 500/550 Mid-Output v2.5 Kit (150 cycles). The targeted enrichment of the dCas9 transcripts was performed separately using an independent probe library and was sequenced together with additional HTO libraries using the Illumina Miseq Reagent Kit v3 (150 cycles).

Computational and statistical analyses

From fastqs to QCed and demultiplexed UMI normalised matrices

FastQC was used to demultiplex the different samples of the three different modalities from the different 10X chip lanes, which each was processed independently. For the cDNA modality, the UMI count matrix was obtained using Cellranger *count*, including the *targeted-panel* argument to get the additional filtered matrices and summary statistics. Cells with less than 500 UMIs per cell or less than 50 genes with at least 1 UMI per cell were discarded. The top 1% cells containing the highest UMI content were also discarded. The expression of all genes across 10X lanes were extremely reproducible (Pearson r = 0.999), showing a ~5-fold UMI count increase in contrast to the non-targeted transcriptome (**Figure S1c**).

For the GDO modality (sgRNAs), Cellranger count was also used using the CRISPR Guide Capture Analysis mode, which uses a Gaussian mixture model to call sgRNA per cell. The cells containing more than one sgRNA were discarded.

To classify each cell into their corresponding CRISPR system of origin (CRISPRi or CRISPRa), both the HTO modality (protein hashes) and the expression of the dCas9 targeted transcript was used. Protein hashes were called using Alevin salmon [12], and the resulting HTO UMI matrix was mixed in with the cDNA matrix containing the expression of the CRISPRi and CRISPRa genes. This matrix was normalised and scaled using Seurat v4 [13] and used to generate a UMAP based on the expression of protein hashes and the dCas9 transcripts expression. Clusters were identified and manually assigned to an HTO category given the expression pattern of each cluster. Finally, the 5% cells classified as CRISPRi that had the lowest expression of CRISPRi transcript were discarded, as well as those 5% of CRISPRa classified cells that had the highest CRISPRi transcript expression. In total, 20,001 (10,647 CRISPRi and 9,354 CRISPRa) cells passed all filters and were used for subsequent analyses.

Once each single cell was classified into a unique sgRNA perturbation and to a cell line of origin, the cDNA UMI matrices of the two 10X lanes were merged and afterwards normalised using a the log1p normalisation method of Seurat's NormalizeData (Seurat version 4.3). On average, each unique sgRNA perturbation was measured in 81 and 86 cells for the CRISPRa and CRISPRi, respectively **(Figure S1d**)

Expression fold-change calculation and non-target sgRNA filtering

As estimates of changes in expression, we used a pseudo-bulk differential analyses approach. To get rid of the batch effects deriving from each cell line (CRISPRa vs. CRISPRa) (**Figure S3a**), for each unique perturbation we calculated log2 fold-change of the of the expression a gene against the expression of that gene in the population of cells harbouring the NTC sgRNAs of that particular cell line. We used Seurat's FindMarkers function to calculate the log2FC and the p-values of a Wilcoxon Rank Sum test.

Before running the differential analyses on all targeted genes, across all unique CRISPR perturbations we identified those NTC sgRNAs that had potential unexpected off target activity and thus could not be used as negative controls. For all possible unique NTC sgRNA pairs we run the above differential expression analysis on all 92 targeted genes. We discarded NTC sgRNAs that showed more than one DE gene (FDR 0.05) in more than one pairwise comparison, and the differential genes showed consistent patterns of change in expression. For this reason, cells harbouring sgRNA NTC_2 on the CRISPRa modality were discarded, as this particular perturbation showed consistent undesired activation of PPP1R14A and CTCFL genes. Additionally, we ran Sceptre [14] using the resulting group of control cells to validate that our samples were calibrated correctly (**Figure S1e**).

Once those potential outlier NTCs were discarded, the log2FC of each targeted gene in each unique sgRNA and cell line condition was calculated. Adjusted FDR p-values were calculated across all tests to later on call significance on DE genes. The obtained fold-changes and FDRs were used for all subsequent analyses.

Linear, loess and sigmoidal model fitting

To identify the best predictive model of each cis-gene dosage to trans-gene fold-change, we fitted three types of models to the data: linear (using the R *lm* function), a four parameter sigmoid (using the *drm(fct = L.4())* function from the R dcr package) and a LOESS fit (R *loess* function). To evaluate and compare the goodness of fit of the linear vs. the sigmoid model taking into account overfitting, we calculated the Akaike information criterion (AIC) using the *AIC* function from the R stats package.

To obtain an accurate prediction of each trans gene expression given TF dosage and avoid overfitting, a 10-fold cross validation scheme was followed by fitting the sigmoid model individually to each curve. The data was randomly split in 10 groups, where 90% of the data was used for training and the remaining 10% for testing. To obtain the values of each individual sigmoid fit for each dosage and trans gene response, the average and standard deviation of each parameter value was calculated across the 10 trained models.

Those trans genes with a slope significantly different from 0 (FDR adjusted p-value of a z-test across the 10 fold-CV parameter outputs) and with a min-to-max range significantly higher than 0.05 (FDR adjusted p-value of a z-test across the difference between the min

and max asymptotes parameters in the 10 fold-CV), were classified as as “responsive” genes. The remaining genes were classified as “unresponsive”. The top 5% trans genes of the GFI1B trans network with the largest ΔRMSE between the LOESS fit and the sigmoid fit ($RMSE_{Sigmoid}$ - $RMSE_{LOESS}$) were classified as non-monotonic and the curve trend manually validated. For the five trans genes classified to have a non-monotonic gene expression response, their predicted expression upon TF dosage change was calculated using the LOESS model instead of the sigmoid one.

Gene-specific properties

Diverse gene annotations and properties were collected to compare with the different *trans* genes response properties (related to Figure 4). Quantitative annotations included the gene biotype(Ensembl [15]), Housekeeping genes [16], transcription factors [4], genes associated with at least one disease (OMIM [17]) and genes associated with blood-related complex traits (obtained from [3]).

Quantitative features included the probability of being loss-of-function intolerant scores (pLI) [18] and synonymous and missense Z scores (mis z) [18,19], which were obtained from the GnomAD database. Haploinsufficiency probability scores were obtained from [20]. To obtain the number of ChIP-Seq peaks of a *cis* gene within the promoter region of trans-genes (n peak [cis gene]), we utilised the regulon generated by Minaeva et al. 2024 [21]. This regulon was created by mapping transcription factor peaks to transcription start sites (TSS) of the 50% expressed isoforms for each gene in K562 cells, with subsequent application of a ±1 Kb proximity filter. Mean expression of genes from bone marrow cell types were obtained from Hay et al. 2018 [22] and averaged across donors. The number of protein-protein interactions of each gene within the entire human proteome (Num PPIs1) was obtained from the STING database [23].

To test significant differences between groups of genes (qualitative features), the Wilcoxon rank test was used. For quantitative features, Pearson correlation between parameters from the sigmoid model with quantitative gene metrics was used. Non-responsive and non-monotonic genes in each trans network were excluded.

Code and data accessibility

All code used in this study is available at https://github.com/LappalainenLab/d2n_ms. Raw sequencing data has been submitted to GEO (accession number GSE257547).

1. Morris, J. A. *et al.* Discovery of target genes and pathways of blood trait loci using pooled CRISPR screens and single cell RNA sequencing. Preprint at https://doi.org/10.1101/2021.04.07.438882.
2. Legut, M. *et al.* High-Throughput Screens of PAM-Flexible Cas9 Variants for Gene

Knockout and Transcriptional Modulation. *Cell Rep.* **30**, 2859–2868.e5 (2020).

3. Morris, J. A. *et al.* Discovery of target genes and pathways at GWAS loci by pooled single-cell CRISPR screens. *Science* **380**, eadh7699 (2023).
4. Garcia-Alonso, L., Holland, C. H., Ibrahim, M. M., Turei, D. & Saez-Rodriguez, J. Benchmark and integration of resources for the estimation of human transcription factor activities. *Genome Res.* **29**, 1363–1375 (2019).
5. McKenna, A. & Shendure, J. FlashFry: a fast and flexible tool for large-scale CRISPR target design. *BMC Biol.* **16**, 74 (2018).
6. Replogle, J. M. *et al.* Mapping information-rich genotype-phenotype landscapes with genome-scale Perturb-seq. *Cell* **185**, 2559–2575.e28 (2022).
7. Xie, S., Armendariz, D., Zhou, P., Duan, J. & Hon, G. C. Global Analysis of Enhancer Targets Reveals Convergent Enhancer-Driven Regulatory Modules. *Cell Rep.* **29**, 2570–2578.e5 (2019).
8. Li, M. *et al.* Regulation of MYB by distal enhancer elements in human myeloid leukemia. *Cell Death Dis.* **12**, 223 (2021).
9. Jost, M. *et al.* Titrating gene expression using libraries of systematically attenuated CRISPR guide RNAs. *Nat. Biotechnol.* **38**, 355–364 (2020).
10. Stoeckius, M. *et al.* Simultaneous epitope and transcriptome measurement in single cells. *Nat. Methods* **14**, 865–868 (2017).
11. Mimitou, E. P. *et al.* Multiplexed detection of proteins, transcriptomes, clonotypes and CRISPR perturbations in single cells. *Nat. Methods* **16**, 409–412 (2019).
12. Srivastava, A., Malik, L., Sarkar, H. & Patro, R. A Bayesian framework for inter-cellular information sharing improves dscRNA-seq quantification. *Bioinformatics* **36**, i292–i299 (2020).
13. Hao, Y. *et al.* Integrated analysis of multimodal single-cell data. *Cell* **184**, 3573–3587.e29 (2021).
14. Barry, T., Wang, X., Morris, J. A., Roeder, K. & Katsevich, E. SCEPTRE improves calibration and sensitivity in single-cell CRISPR screen analysis. *Genome Biol.* **22**, 344

(2021).

15. Martin, F. J. *et al.* Ensembl 2023. *Nucleic Acids Res.* **51**, D933–D941 (2023).
16. Eisenberg, E. & Levanon, E. Y. Human housekeeping genes, revisited. *Trends Genet.* **29**, 569–574 (2013).
17. Amberger, J. S., Bocchini, C. A., Schiettecatte, F., Scott, A. F. & Hamosh, A. OMIM.org: Online Mendelian Inheritance in Man (OMIM®), an online catalog of human genes and genetic disorders. *Nucleic Acids Res.* **43**, D789–98 (2015).
18. Lek, M. *et al.* Analysis of protein-coding genetic variation in 60,706 humans. *Nature* **536**, 285–291 (2016).
19. Samocha, K. E. *et al.* A framework for the interpretation of de novo mutation in human disease. *Nat. Genet.* **46**, 944–950 (2014).
20. Collins, R. L. *et al.* A cross-disorder dosage sensitivity map of the human genome. *Cell* **185**, 3041–3055.e25 (2022).
21. Minaeva, M., Domingo, J., Rentzsch, P. & Lappalainen, T. Specifying cellular context of transcription factor regulons for exploring context-specific gene regulation programs. *bioRxiv* 2023.12.31.573765 (2024) doi:10.1101/2023.12.31.573765.
22. Hay, S. B., Ferchen, K., Chetal, K., Grimes, H. L. & Salomonis, N. The Human Cell Atlas bone marrow single-cell interactive web portal. *Exp. Hematol.* **68**, 51–61 (2018).
23. Szklarczyk, D. *et al.* STRING v10: protein-protein interaction networks, integrated over the tree of life. *Nucleic Acids Res.* **43**, D447–52 (2015).

Main Figures

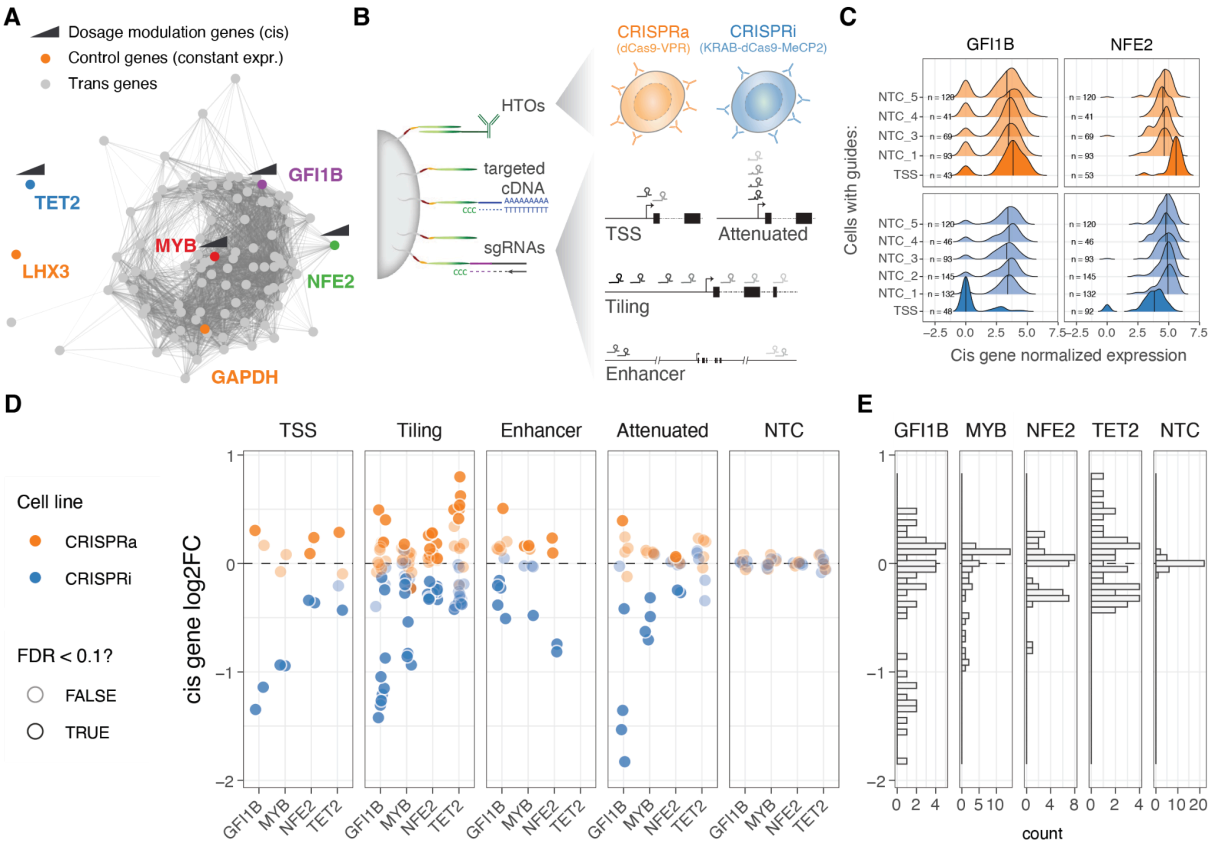

Figure 1: Modulation and quantification of gene dosage using CRISPR and targeted multimodal single-cell sequencing.

A. Co-expression network representation of the 92 selected genes under study. Genes (nodes) are connected by edges when their co-expression across single cells was above 0.5 (data used from Morris *et al*. 2023). Highlighted in colour are the two control highly (GAPDH) and lowly (LHX3) constantly expressed genes, as well as cis genes for which dosage was modulated with CRISPRi/a.

B. Design of the multimodal single cell experiment (HTO = hash-tag oligos).

C. Distribution of the GFI1B (left) or NFE2 (right) normalised expression across single cells for different classes of sgRNAs (NTC = Non-targeting controls, TSS = transcription start site).

D. Resulting relative expression change (log2 fold change) of the 4 cis genes upon each unique CRISPR perturbation when grouped across different classes of sgRNAs.

E. Distribution of cis gene log2FC across all sgRNA perturbations.

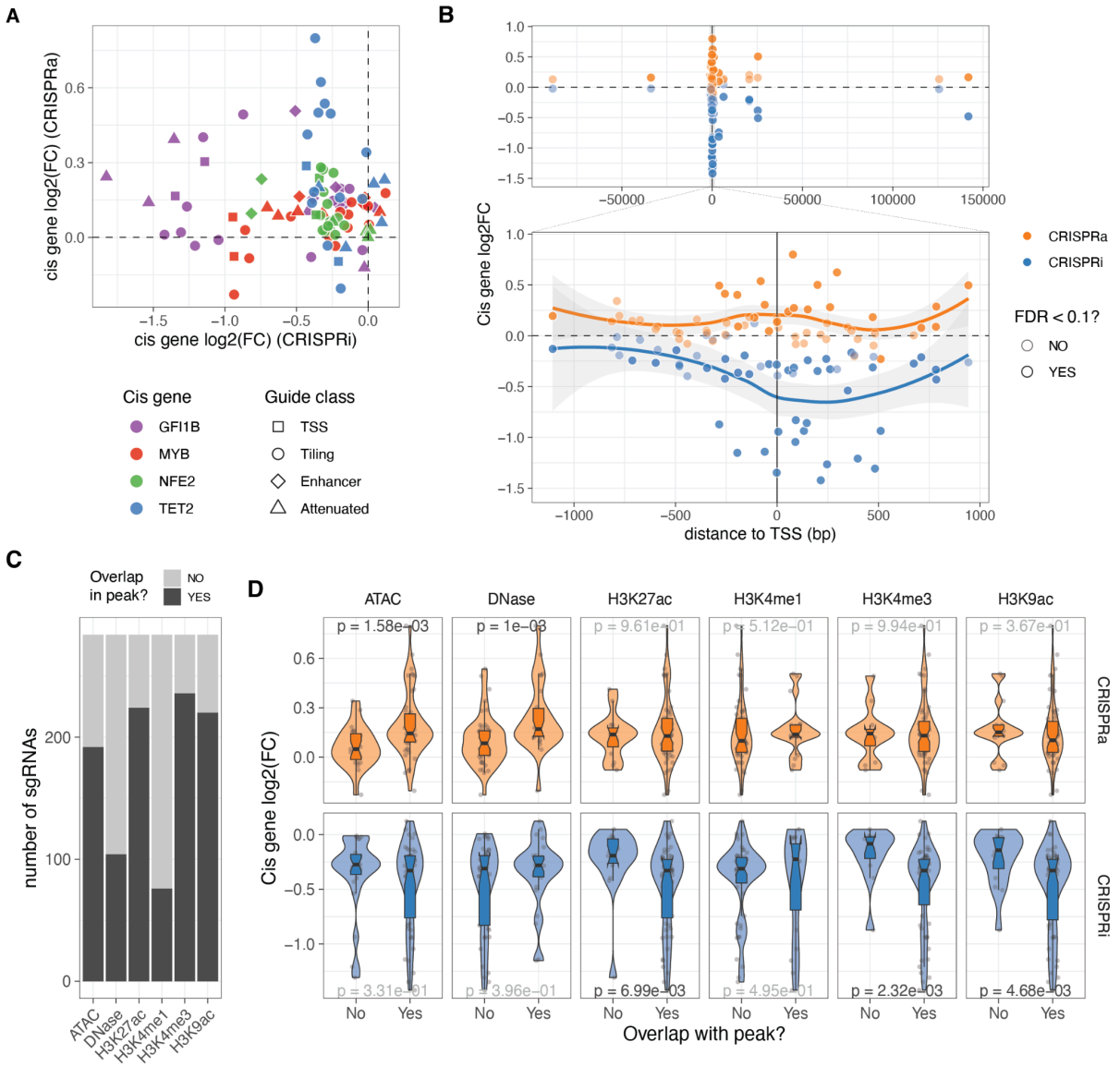

Figure 2: Cis determinants of dosage.

A. Comparison of the relative expression change (log2FC) from the same sgRNA between the two different CRISPR modalities.
B. Relative expression change of the targeted cis gene based on distance from transcription start site (TSS). Top plot excluded attenuated and NTC sgRNAs, while bottom plot also excludes enhancer sgRNAs.
C. Number of sgRNAs that overlap with the different epigenetic or open chromatin peaks.
D. Relative expression change to NTC sgRNAs (log2(FC)) of all cis genes when their sgRNAs fall or not in the different epigenetic or open chromatin peaks. P-value result from Wilcoxon rank-sum tests, with nominally significant p-values shown in black.

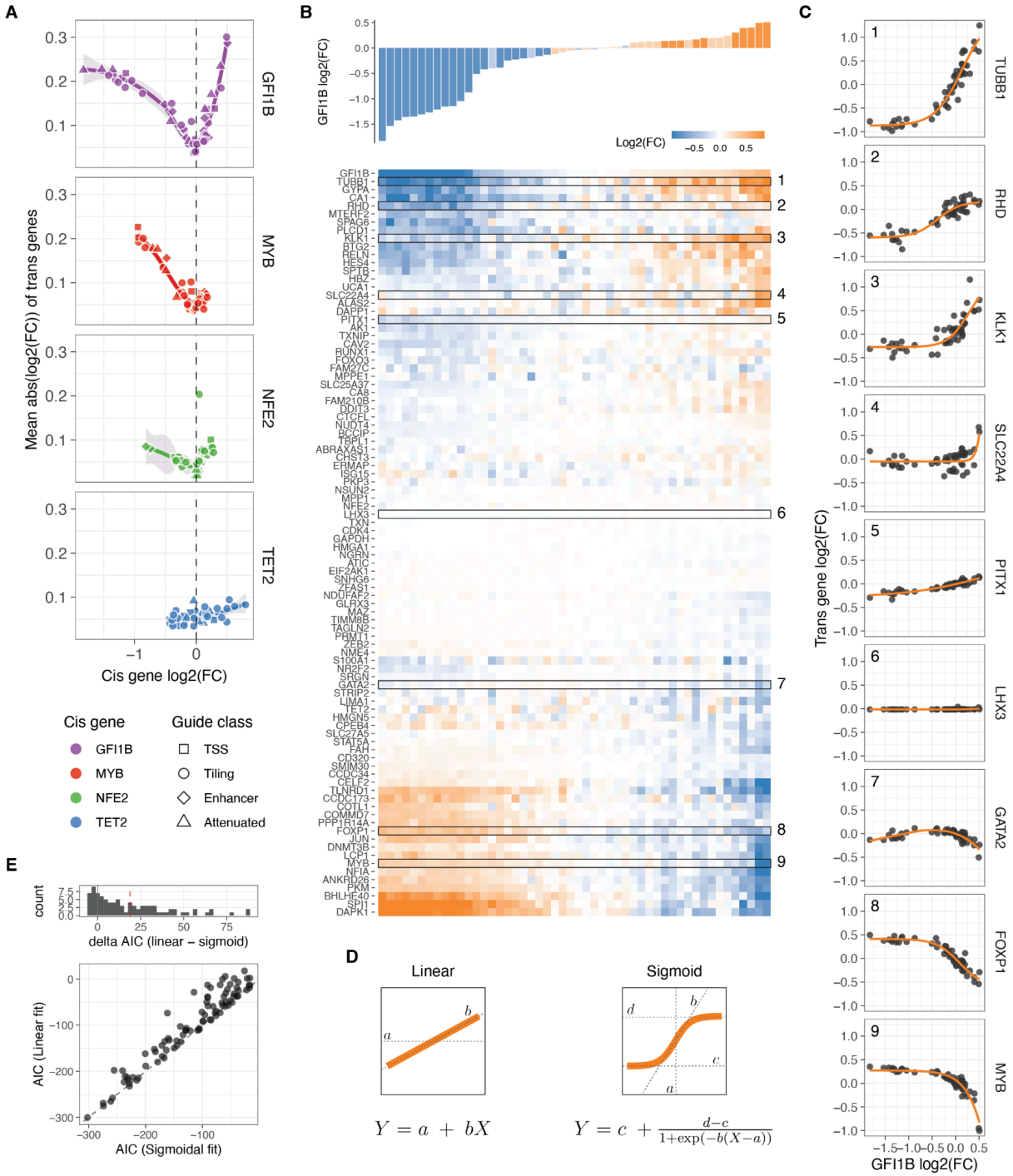

Figure 3: Trans responses of transcription factor dosage modulation

A. Average absolute expression change of all trans genes relative to the changes in expression of the cis genes.

B. Changes in relative expression of all trans genes (bottom heatmap) in response to GFI1B expression changes (top barplot) upon each distinct targeted sgRNA perturbation. The rows of the heatmap (trans genes) are hierarchically clustered based on their expression fold change linked to alterations in GFI1B dosage.

C. Dosage response curves of the highlighted trans gene in B as a function of changes in GFI1B expression. The orange line represents the sigmoid model fit, except for GATA2, which display a non-monotonic response and are fitted with a loess curve.

D. Illustration of the linear and sigmoid models and equations used to fit the dosage response curves.
E. Distribution of the difference in Akaike Information Criterion ($\Delta AIC_{linear\text{-}sigmoid}$) after fitting the sigmoidal or linear model for each trans gene upon GFI1B dosage modulation (top panel), and the direct comparison of the AIC of each fit (bottom panel).

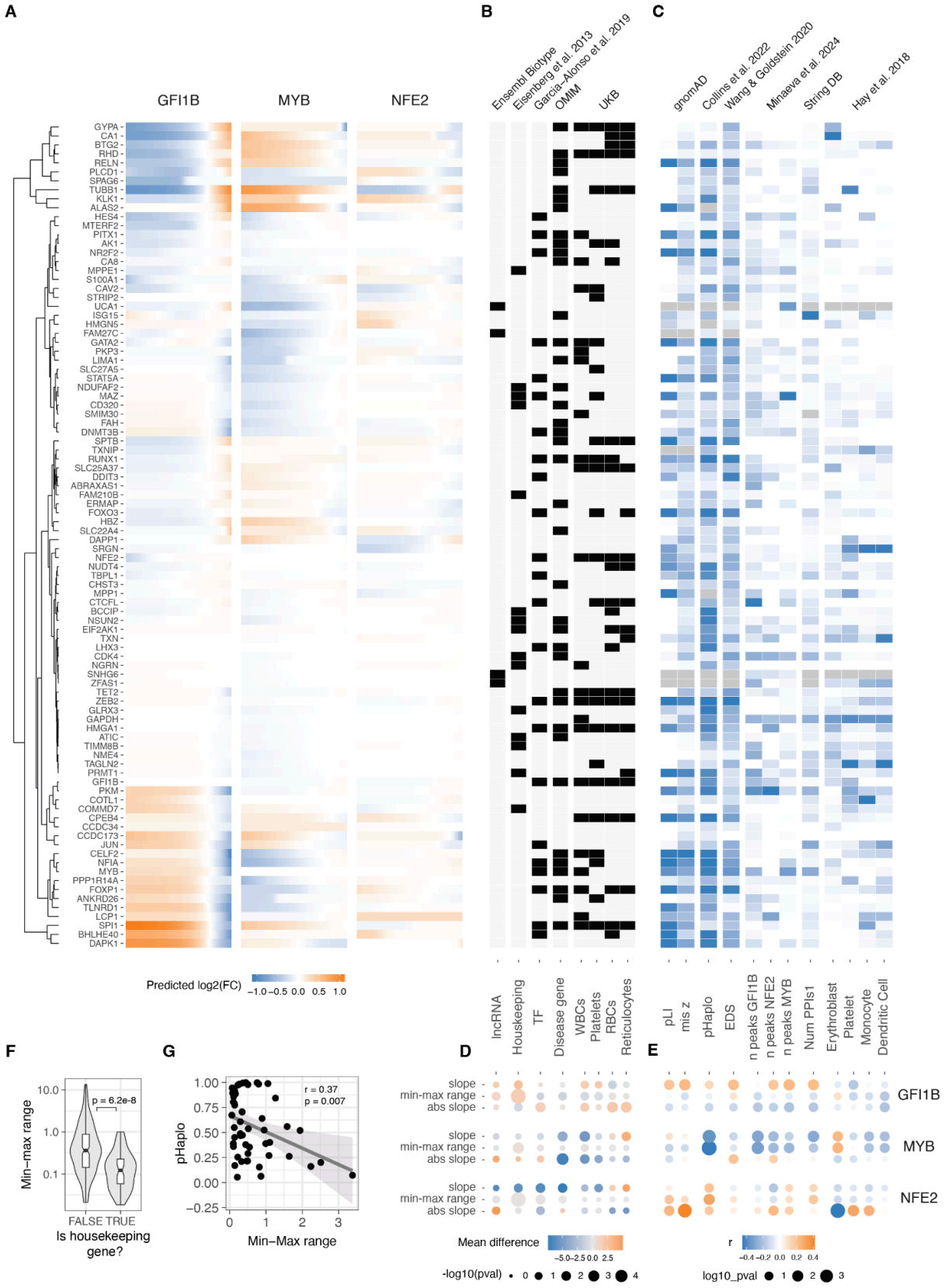

Figure 4: Relationship between gene and dosage response properties

A. Predicted changes (using sigmoid or loess fits for monotonic and non-monotonic responses, respectively) in relative expression of all trans genes in response to changes of the GFI1B, MYB and NFE2 expression. Trans genes (rows) were

hierarchically clustered based on their expression fold change linked to alterations of all TF's dosage. Dendrogram of the resulting clustering shown in the left.

B. Heatmap highlighting the qualitative gene features of each transgene. X axis indicates the gene property and top subtitles indicate where the data was obtained from. Grey indicates missing data.
C. Heatmap indicating the z-scaled quantitative gene features of each transgene. X axis indicates the gene property and top subtitles indicate where the data was obtained from. Grey indicates missing data.
D. Difference in the average value of the sigmoid parameter indicated in right between the genes qualified into the no/yes category of the gene properties indicated in B.
E. Pearson correlation coefficient of the quantitative trans gene features (shown in C) with the sigmoid parameter value for each transgene in the response of the modulation of dosage of the TF indicated on the left. Size of the points are inversely related to significance of correlation, and colour indicates the direction of correlation.
F. Differences in the range of expression response for Housekeeping vs. non-Housekeeping transgenes with changes of dosage of MYB, GFI1B and NFE2.
G. Negative correlation between haploinsufficiency score (pHaplo) and the range of the response of transgenes to the modulation of MYB.

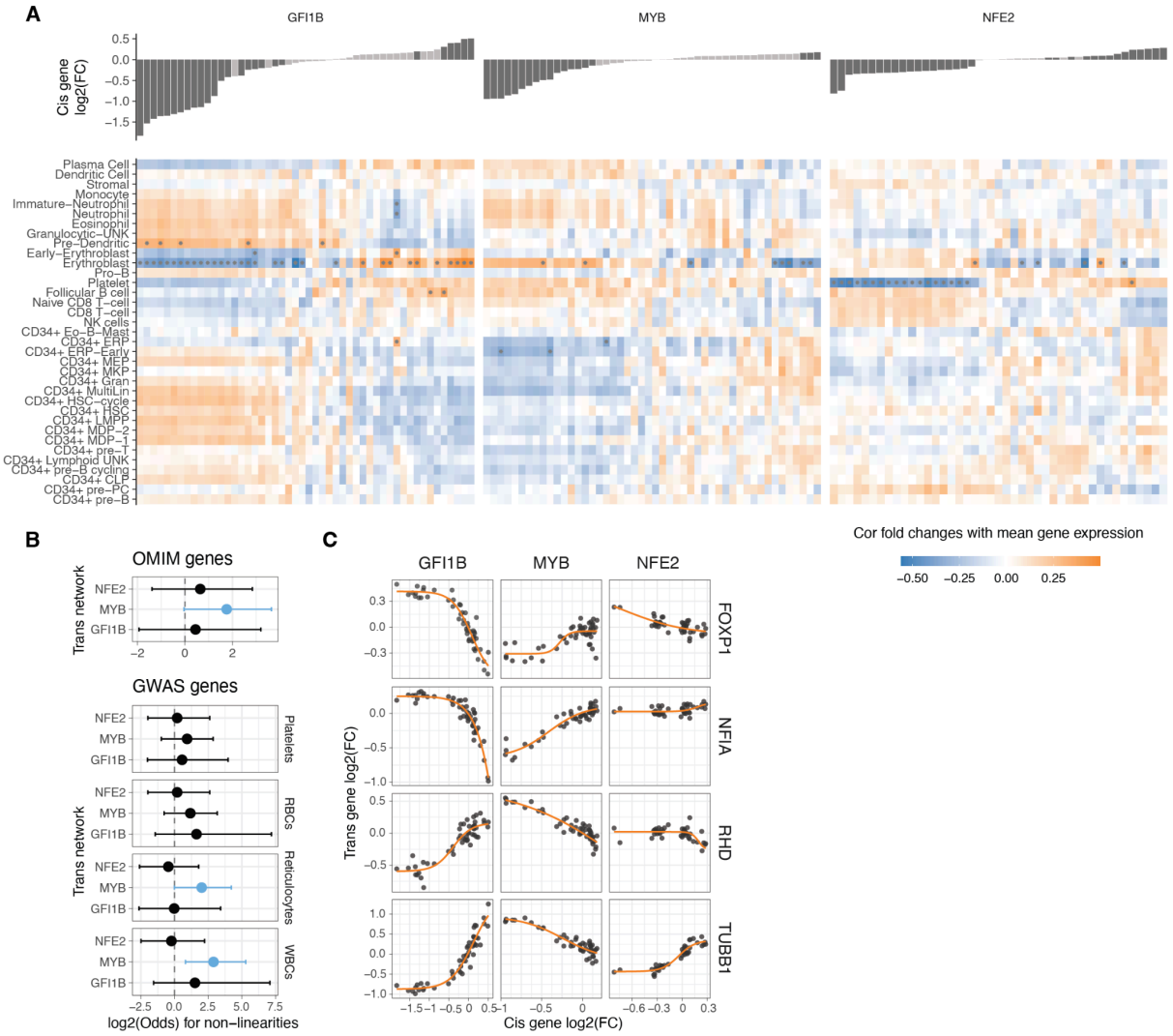

Figure 5: Non-linearities in TF dosage responses of complex traits and disease genes

A. Heatmap illustrating the correlation between the mean expression of cell types and the changes in expression linked to individual TF dosage perturbations. The barplot on the top panel represents cis gene dosage perturbation. Asterisks (*) denote correlations with 10% FDR.

B. Enrichment log(odds) ratio of non-linear TF dosage responses ($\Delta AIC_{linear\text{-}sigmoid} > 0$) in disease related genes (OMIM genes linked to 1 or more diseases, top panel) or in GWAS blood traits associated genes (closest expressed gene to lead GWAS variant, bottom panel). Log(odds) with Fisher's exact test at FDR < 0.05 are highlighted in blue.

C. Examples of TF dosage response curves of genes both associated with disease (OMIM) and complex traits (Blood GWAS).

Supplementary Figures

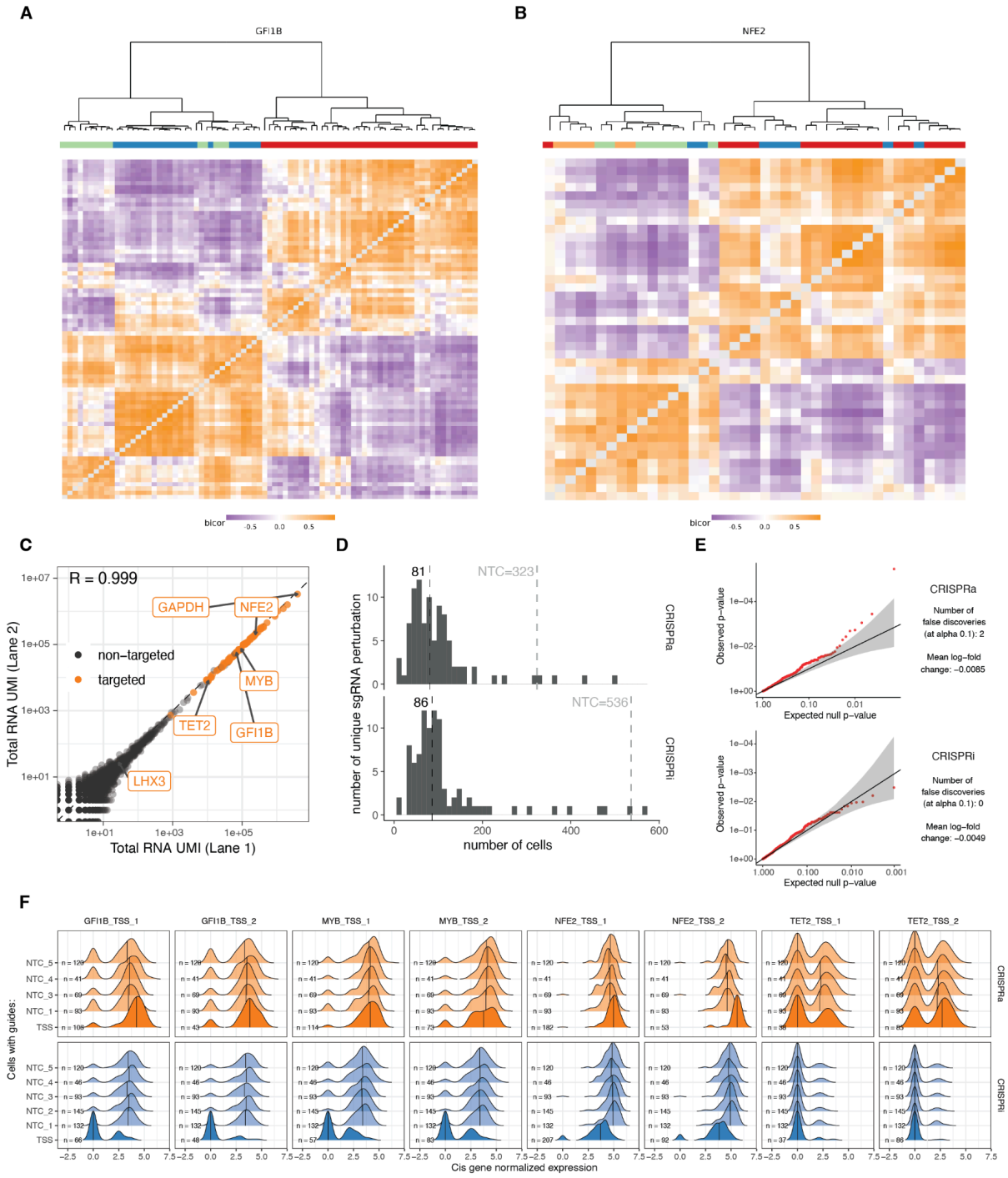

Figure S1: Experimental design and data processing from UMIs to expression fold-change, related to Figure 1 and STAR methods.

A. Co-expression matrix of the 76 selected GFI1B trans genes based on K562 data from [1]. Three clusters from the selected targeted panel show similar co-expression architecture than the original clusters identified using the entire GFI1B trans-network (original clusters A in blue, B in green and C in red).

B. Same as (A) for the 39 NFE2 trans genes (original clusters A in green, B in orange, C in blue and D in red).
C. Correlation between total UMI counts per gene between 10X chip lanes. Targeted panel genes are shown in orange and highlighted names correspond to dosage genes (NFE2, MYB, GFI1B and TET2) and low/high expression controls (LHX3 and GAPDH).
D. The number of singlet cells carrying each sgRNA in the two different CRISPR cell lines. NTC = non-targeting controls.
E. Q-Q plots from Sceptre calibration test.
F. Distribution of normalised UMI expression of the cis gene labelled on top for cells with sgRNAs targeting their TSS or harbouring NTC sgRNAs.

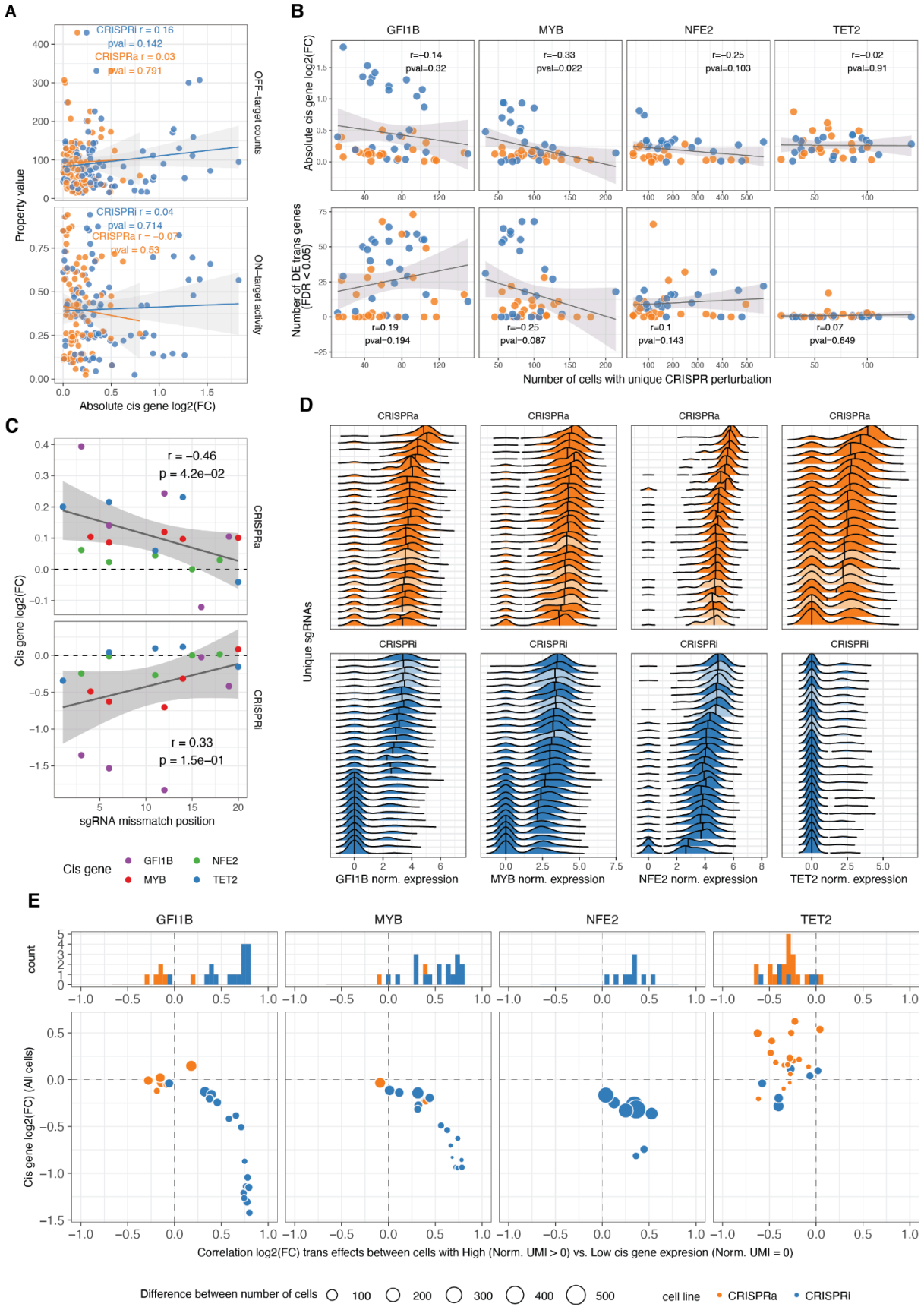

Figure S2: Biochemical and activity properties of different types of sgRNAs

A. Relationship between off-target and on-target activity of sgRNAs and the change in expression of their target cis gene.
B. Relationship between the number of cells that covered each sgRNA perturbation with the absolute fold change of the cis gene (top) or the number of differentially expressed trans genes due to the cis gene perturbation (bottom).
C. Relationship between the location of the mismatch mutation of attenuated sgRNAs (position 1 being farthest away from PAM motif location) and their effect on the cis gene expression.
D. Distribution of the normalised cis gene UMIs in single cells, grouped by their unique sgRNAs, ranked top to bottom by mean normalised expression. Transparent distributions correspond to non-targeting controls.
E. Distribution of the correlation in trans gene expression fold-changes when splitting the same sgRNA cells into 0 UMI or >0 UMI for the cis gene (top panel). Comparison of the strength of these correlations with the effect of that sgRNA on the cis gene (bottom panel). Size of dots indicate the difference in the size of the 0 UMI or >0 UMI cell groups.

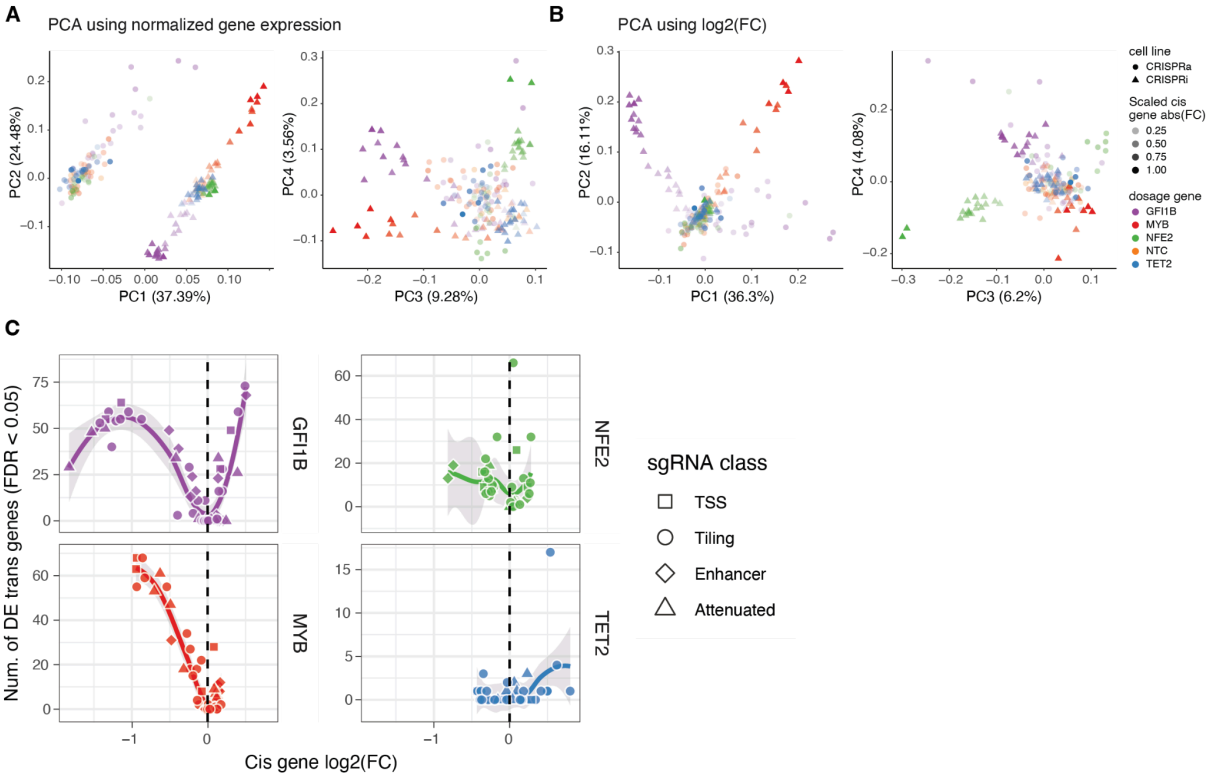

Figure S3: Global view of trans effects when modulating TF dosage

A. PCA of mean UMI normalised expression (not relative to each cell line of origin) for all genes across unique sgRNA perturbations.
B. Same as A but using relative expression fold-change when normalising by the CRISPR cell line of origin.
C. Number of differentially expressed trans genes relative to the cis gene dosage perturbation.

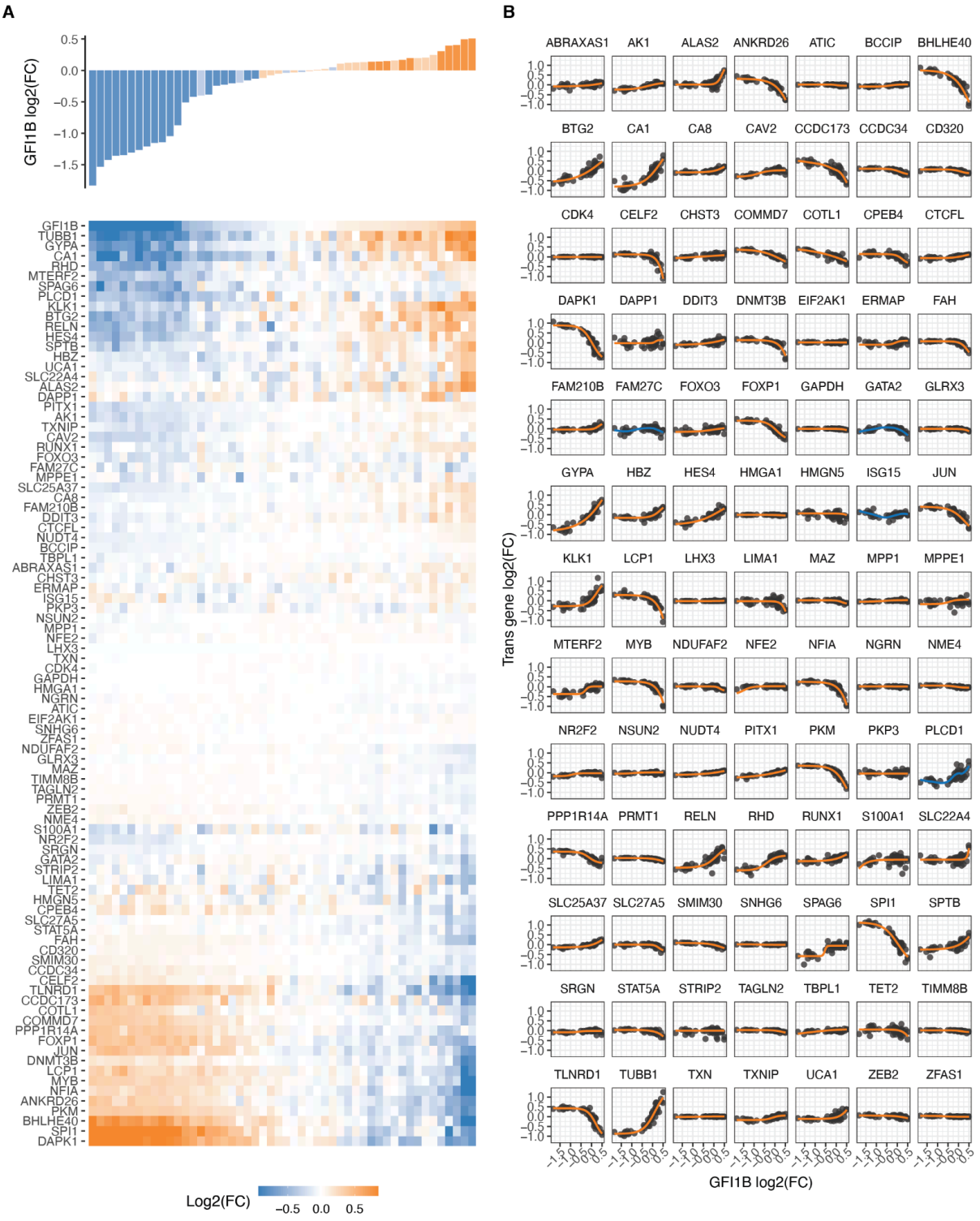

Figure S4: Transgenes responses to GFI1B dosage modulation

A. Changes in relative expression of all trans genes (heatmap) in response to GFI1B expression (top barplot) upon each distinct targeted sgRNA perturbation. The rows of the heatmap (trans genes) are hierarchically clustered based on their expression fold change linked to alterations in GFI1B dosage.

B. Dosage response curves are plotted for each trans gene against changes in GFI1B expression. The orange line represents the sigmoid model fit, and the blue line represents a loess curve.

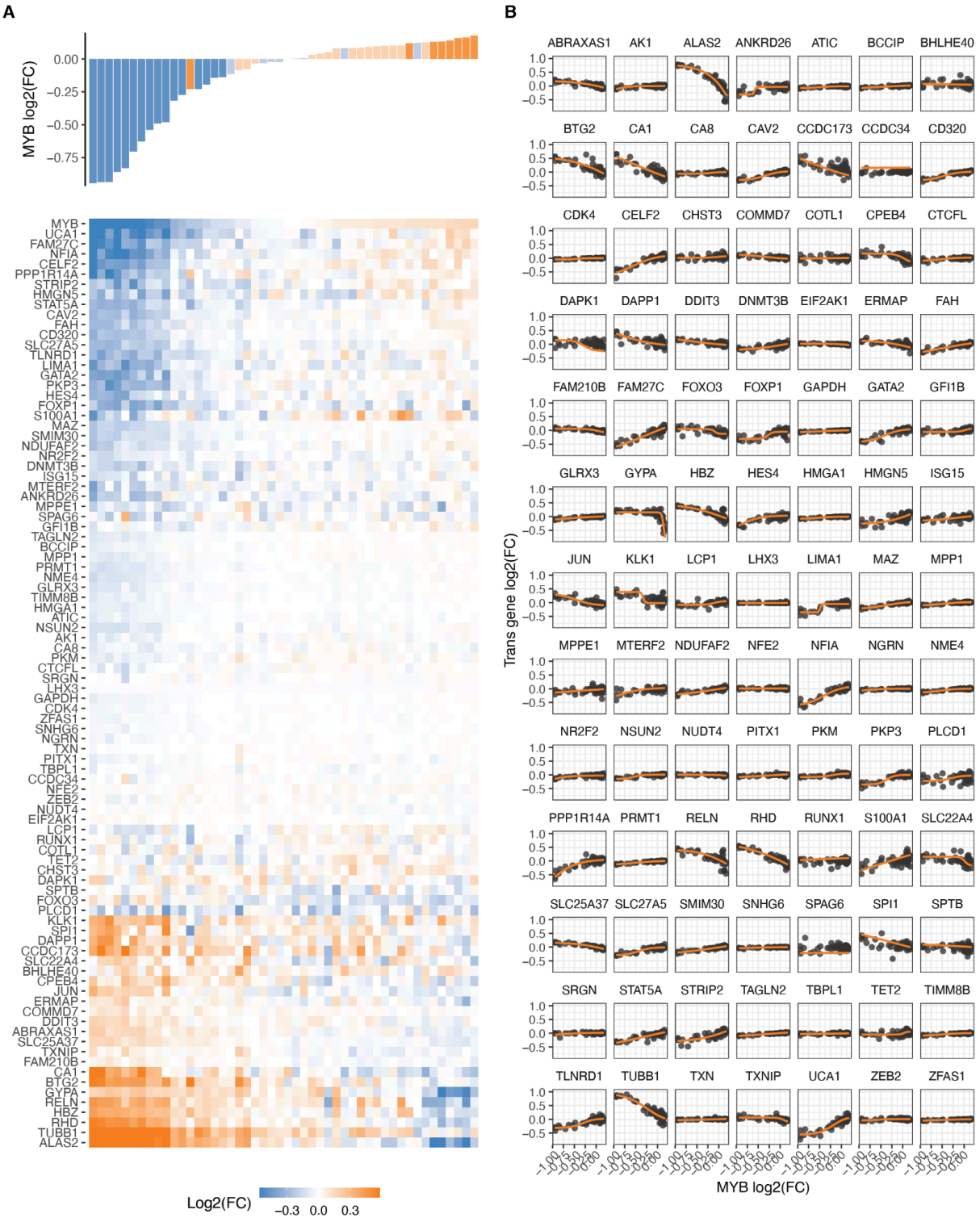

Figure S5: Transgenes responses to MYB dosage modulation

A. Changes in relative expression of all trans genes (bottom heatmap) in response to MYB expression (top barplot) upon each distinct targeted GFI1B sgRNA perturbation. The rows of the heatmap (trans genes) are hierarchically clustered based on their expression fold change linked to alterations in MYB dosage.

B. Dosage response curves are plotted for each trans gene against changes in MYB expression. The orange line represents the sigmoid model fit.

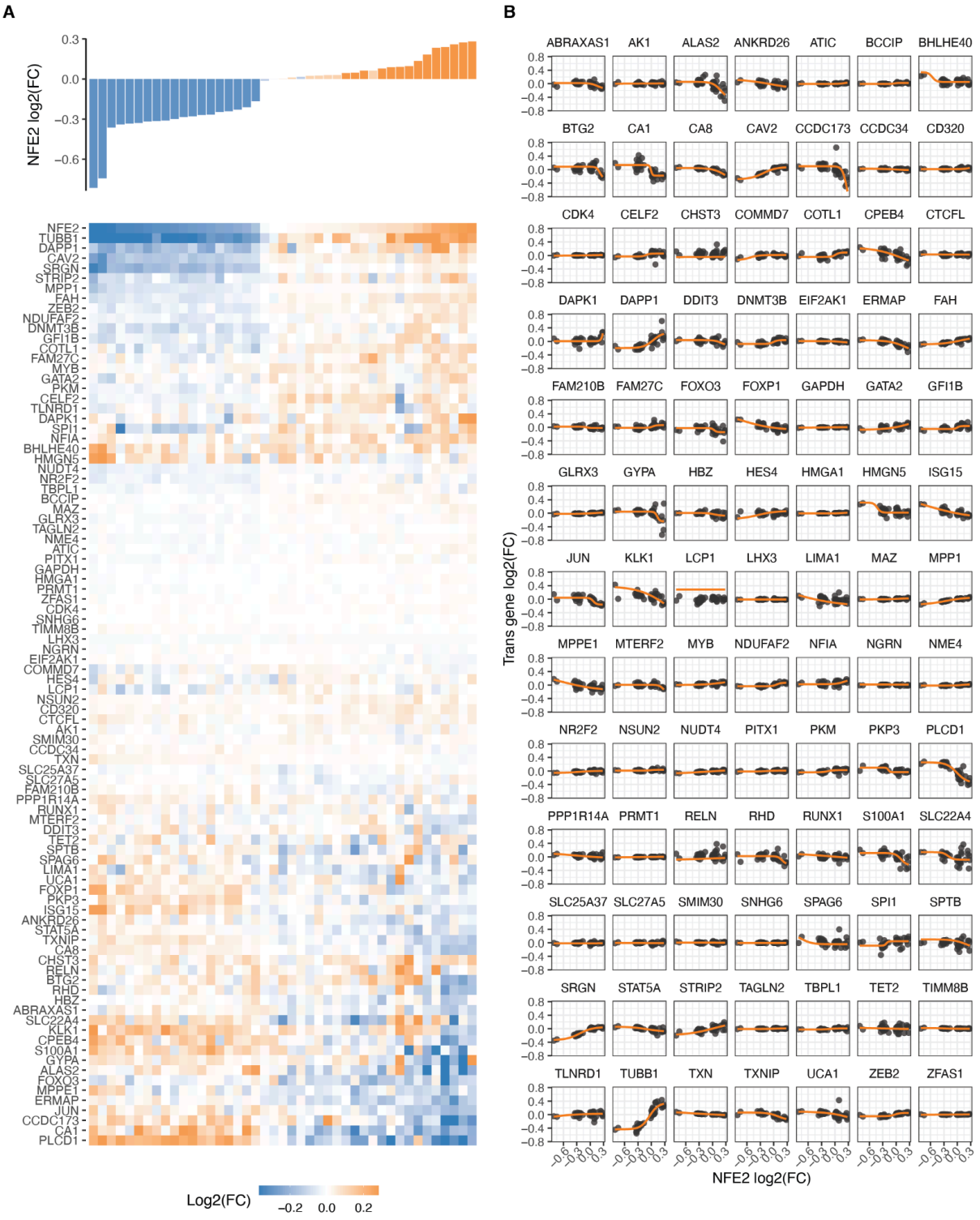

Figure S6: Transgenes responses to NFE2 dosage modulation

A. Changes in relative expression of all trans genes (bottom heatmap) in response to NFE2 expression (top barplot) upon each distinct targeted NFE2 sgRNA perturbation. The rows of the heatmap (trans genes) are hierarchically clustered based on their expression fold change linked to alterations in NFE2 dosage.

B. Dosage response curves are plotted for each trans gene against changes in NFE2 expression. The orange line represents the sigmoid model fit.

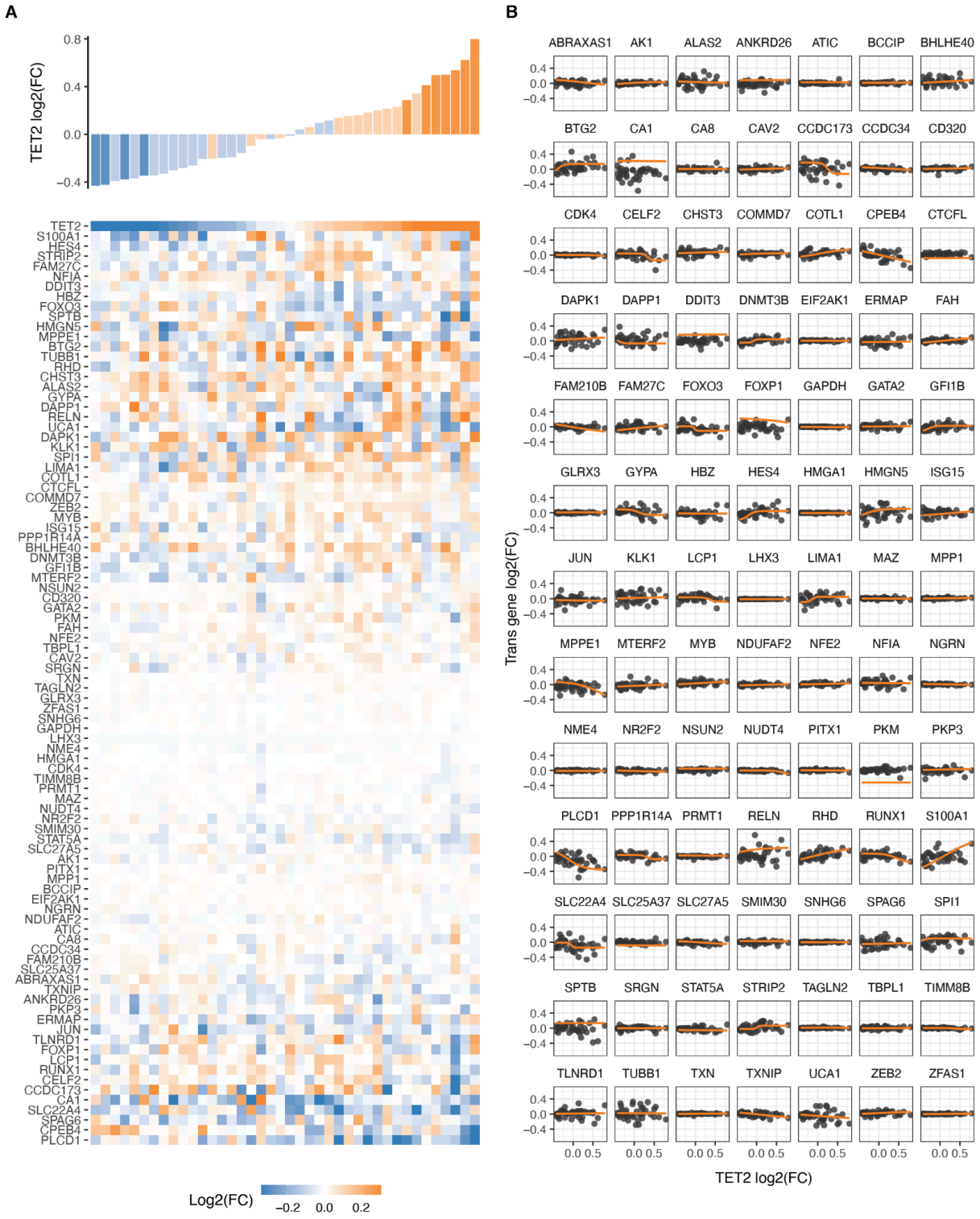

Figure S7: Transgenes responses to TET2 dosage modulation

A. Changes in relative expression of all trans genes (bottom heatmap) in response to TET2 expression (top barplot) upon each distinct targeted TET2 sgRNA perturbation. The rows of the heatmap (trans genes) are hierarchically clustered based on their expression fold change linked to alterations in TET2 dosage.

B. Dosage response curves are plotted for each trans gene against changes in TET2 expression. The orange line represents the sigmoid model fit.

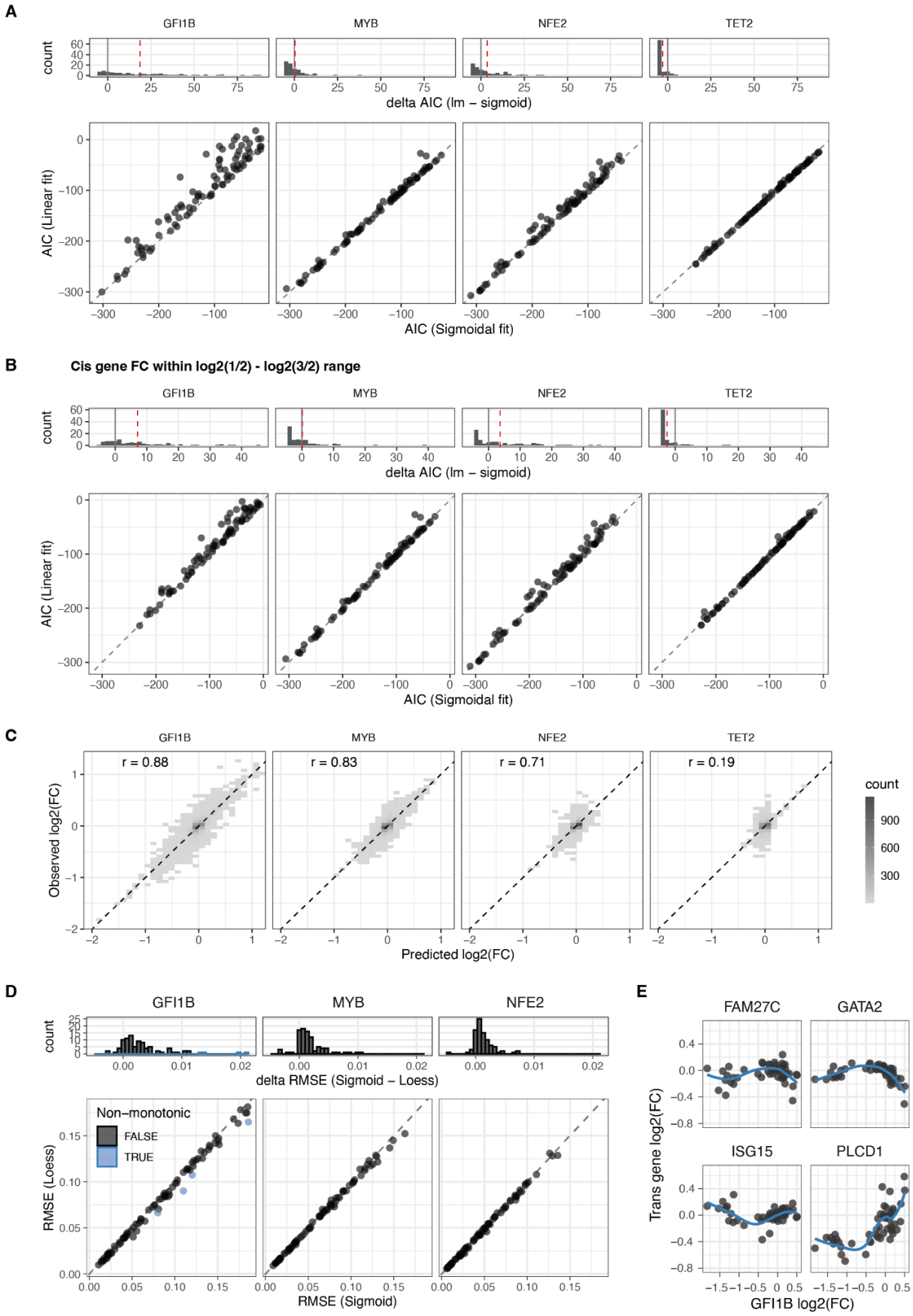

Figure S8: Dosage response linear and non-linear model fitting

A. Distribution of the difference in Akaike Information Criterion ($\Delta AIC_{linear\text{-}sigmoid}$) after fitting the sigmoidal or linear model for each trans gene based on the gradual expression perturbations of the four cis genes (top panel), and the direct comparison of the AIC of each fit (bottom panel).
B. Same as A but only fitting the models on those sgRNA perturbations that lead to a cis gene dosage change bounded between log2(1/2) and log2(3/2).
C. Agreement between observed and predicted trans genes expression fold change upon cis gene dosage modulation across a 10-fold cross-validation scheme.
D. Comparison of the Root Mean Square Error (RMSE) of the sigmoid model on the different trans genes dosage responses to the RMSE of the equivalent loess fit (bottom panel). In blue are highlighted the non-monotonic responses that correspond to the top four $\Delta RMSE_{sigmoid\text{-}loess}$ ($RMSE_{sigmoid}$ - $RMSE_{loess}$) values (top panel).

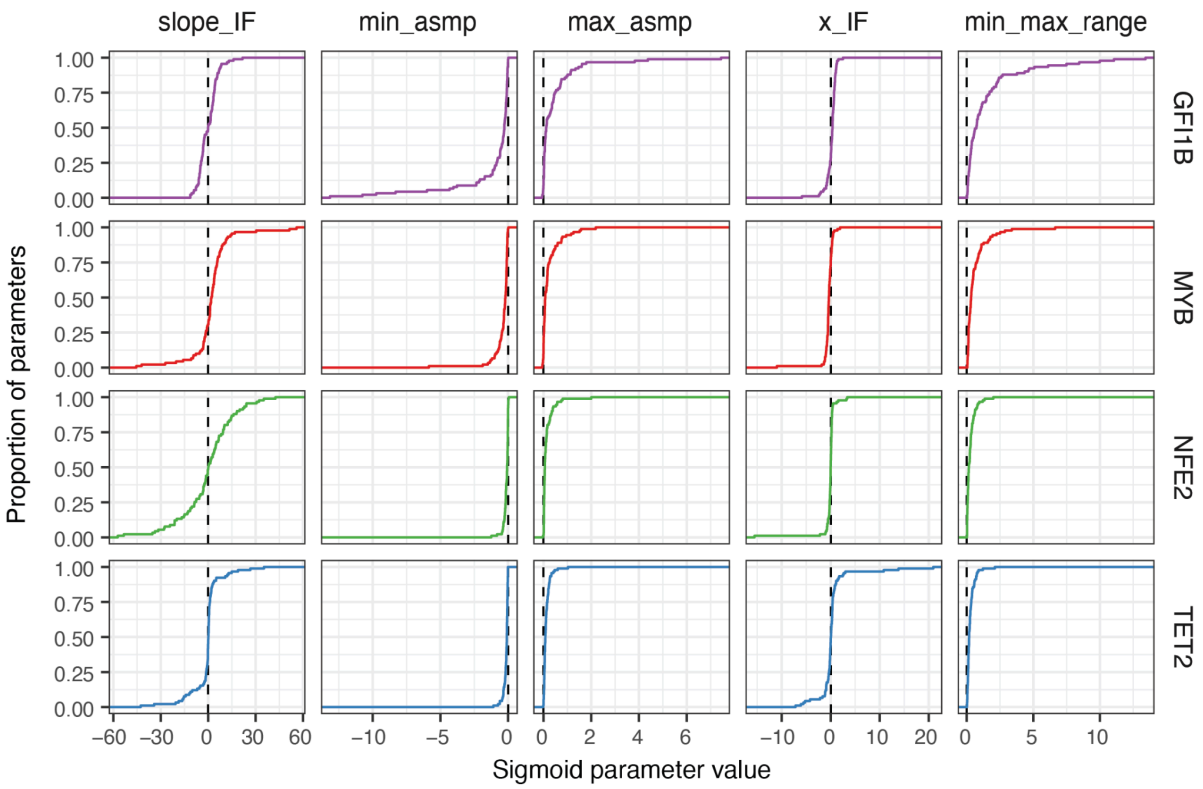

Figure S9: Distribution of the fitted parameters of sigmoidal model on dosage responses

Cumulative distribution of the four fitted parameters (first four columns) of the sigmoid model across genes given the independent perturbation of the four TFs (rows). slope_IF = slope of dosage response curve at the inflection point, min_asmp = minimum asymptote (minimum trans gene dosage level), max_asmp = maximum asymptote (maximum trans gene dosage level), x_IF = TF expression FC at the dosage response inflection point.

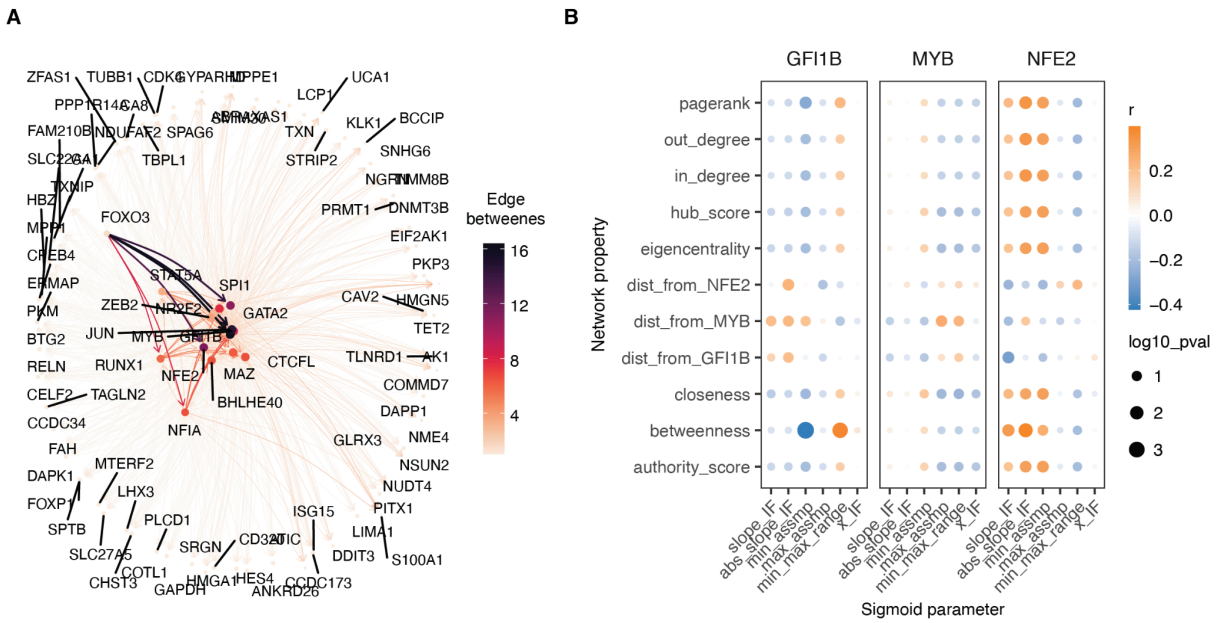

Figure S10: Relationship gene properties and TF-target network properties with TF dosage responses

A. A regulatory network constructed based on TF-target gene data Minaeva et al. 2024 with nodes and edges coloured by betweenness. Nodes are sized by their degree.

B. Heatmap illustrating the correlation between the sigmoid parameters in response to cis-gene modulation and network centrality metrics calculated based on the regulatory networks from Minaeva et al. 2024. Point size is scaled to -log10 p-value.

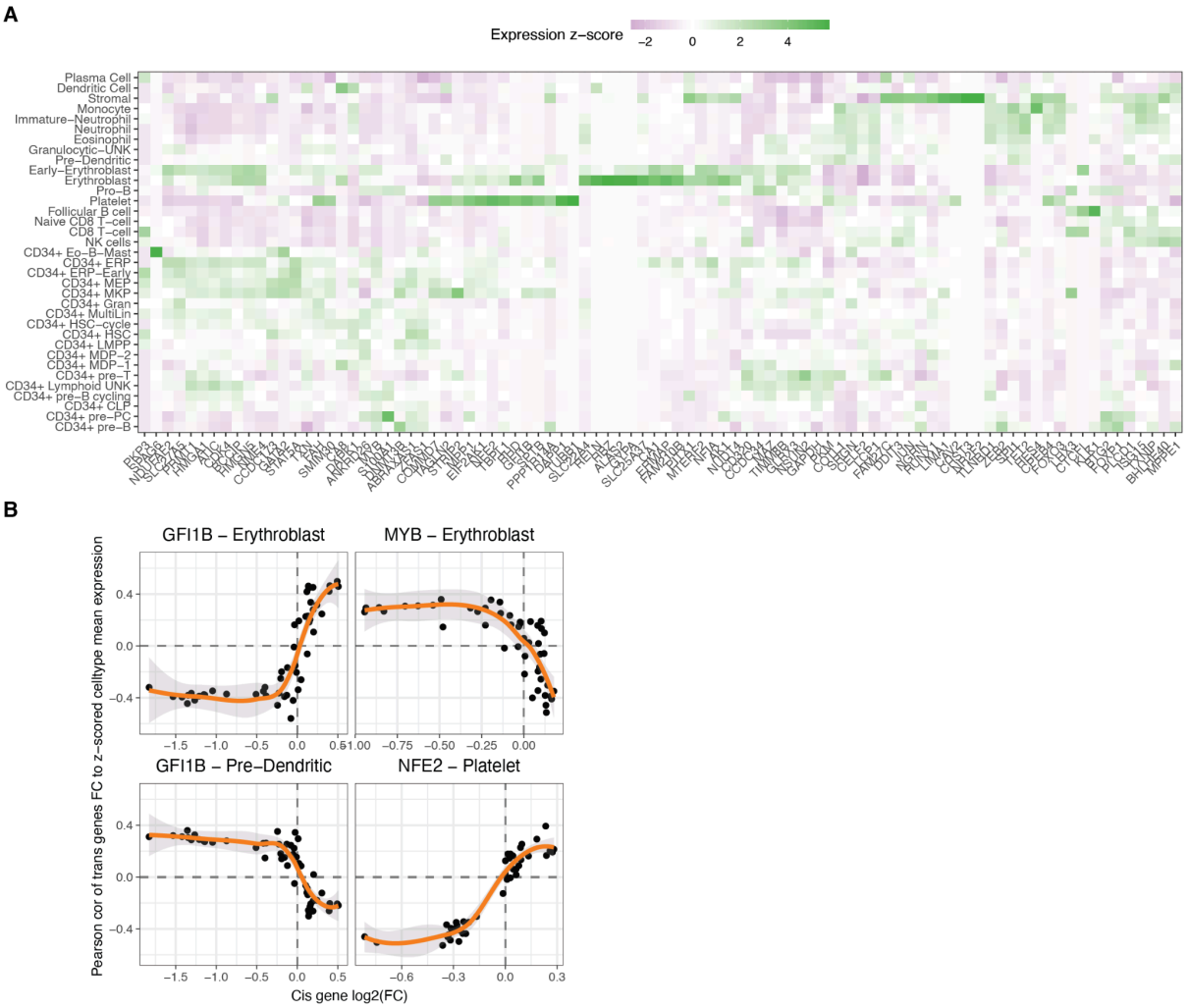

Figure S11: Transcriptional similarity among bone marrow cell types at different TF dosage levels

A. Normalised z-score mean expression across donors for targeted genes within each bone marrow cell type (Data from the Human Cell Atlas).

B. Examples of trends of correlation of transgenes expression with the TF change in dosage. The title specifies the cis gene and the cell type for which the trans effects of TF dosage modulation have been contrasted to.